AN EXPERIMENTAL INVESTIGATION OF THE PRESSURE DISTRIBUTION OF AIR IN RADIAL FLOW IN THIN FILMS BETWEEN PARALLEL PLATES

PHILIP F. CAROTHERS, JR.

AN EXPERIMENTAL INVESTIGATION OF THE PRESSURE DISTRIBUTION OF AIR IN RADIAL FLOW IN THIN FILMS BETWEEN PARALLEL PLATES

****

Philip F. Carothers, Jr.

AN EXPERIMENTAL INVESTIGATION

OF THE PRESSURE DISTRIBUTION OF

AIR IN RADIAL FLOW IN THIN FILMS

by

Philip F. Carothers, Jr.

This work is accepted as fulfilling the thesis

requirements for the degree of

MASTER OF SCIENCE

IN

MECHANICAL ENGINEERING

from the

United States Naval Postgraduate School

AN EXPERIMENTAL INVESTIGATION OF THE PRESSURE DISTRIBUTION OF AIR IN RADIAL FLOW IN THIN FILMS BETWEEN PARALLEL PLATES

by

Philip F. Carothers, Jr.
Lieutenant, United States Navy

Submitted in partial fulfillment of
the requirements for the degree of

MASTER OF SCIENCE

IN

MECHANICAL ENGINEERING

United States Naval Postgraduate School
Monterey, California

1961

Abstract

An experimental investigation of the pressure distribution of air in radial flow between parallel plates was conducted.

Data were collected on the pressure distribution, mass rate of flow of air and film thickness.

Variations were made in the load applied to the upper plate, stagnation pressure at the air supply hole, and the upper plate geometry. Two upper plates having the same outside diameters but different supply hole diameters were employed.

Two flow regimes were defined, that where the flow of air is dominated by the viscous forces wherein the pressure decreases steadily from the supply hole to the outer edge of the upper plate and that where the inertia forces predominate and the flow becomes supersonic near the air supply hole. In this latter regime, it was found that the mass flow can be predicted by the theoretic choked flow through the cylindrical area defined by the film thickness and the diameter of the air supply hole.

Acknowledgement

Part of this investigation was completed during the writer's stay at the International Business Machines Research Laboratory in San Jose, California. The writer wishes to express his appreciation to Dr. W.A. Gross for making this visit possible.

Thanks are also due to Prof. P.F. Pucci, thesis advisor, whose courtesy, help and guidance made the completion of this thesis possible.

A word of appreciation is due here to my wife, Nancy, for her help with typing and grammar.

Table of Contents

Notation

d_o = Diameter of the air supply hole in the upper plate

F = Force

h = Film Thickness

$\dot{m}$ = Mass rate of flow

P_a = Ambient Pressure

P = Pressure at any point in film

P_o = Stagnation pressure

r = Any radial location under the upper plate

r_o = Radius of the air supply hole in the upper plate

R_1 = Outer radius of the upper plate

T = Temperature

1. Introduction

One of the basic problems of machine design is the support of moving elements. In the past, many familiar devices such as hydrodynamic bearings, ball and roller bearings have been used to solve this problem. The usual lubricant used has been a liquid.

There is a large class of lubrication problems for which hydrodynamic (self-acting) bearings can not be used. These are cases where loads are too high for hydrodynamic bearings to support or where it is essential to avoid contact between bearing surfaces. The solution to this problem is the hydrostatic, or externally pressurized bearing.

The hydrostatic bearing has become of interest not only in satisfying the above requirements, but also because of its low friction with high speed shafts and because of the need to support heavy non-rotating elements. Again, the most common lubricant has been a liquid.

The use of a gas for bearing lubrication was first suggested by Hirn[1] in 1855.[1] About forty years later Kingsbury [2] tested a hydrodynamically lubricated air bearing and reported the results.

1. Numbers in brackets refer to references listed in the Bibliography.

Air as a lubricant has several advantages. Chief among these are its viscosity characteristic and its availability. The viscosity of air is several orders of magnitude lower than that of greases or oils. This results in extremely low starting and running torques. The viscosity of air, as is typical of gases, increases with temperature. This becomes important if bearings are to be operated at temperatures of 1000°F or more. [3]

The externally pressurized or hydrostatic air bearing combines the several features, described above, of the hydrostatic bearing together with the desirable lubricant, air.

The circular pad bearing shown schematically in Figure 1, is of interest both as a thrust bearing and because it can be considered to be the basic unit of a journal bearing.

The gas dynamics of the flow of air through the centrally fed pad bearing is the analysis of radial flow between parallel plates. The analysis can be separated into essentially two flow regimes under certain conditions of supply pressure and loading the radial flow is dominated by the viscous forces and hence, the radial pressure distribution is one which gradually decreases from the central supply pressure to ambient pressure at the outer radius.

Many investigations of the flow in this viscous regime have been performed, notable among these is the work of Laub [4] , Gross [5] , and Comolet [6] .

Under other conditions, however, fluid inertia forces are significant and supersonic flow in a portion of the radial flow exists. To satisfy the boundary conditions imposed upon the flow, discontinuities in the flow in the form of shocks appear. Since the flow is also influenced signifigantly by the fluid viscosity, interactions between the shock(s) and viscous effects occur, and depending upon the supply pressure and loading this interaction can occur in extremely short radial distances or can be distributed over a significant radial distance.

This regime has been recognized by several investigators and an analytic treatment of this regime was attempted by Mori [7] . Lack of sufficient, good, experimental data prevented Mori and other previous investigators from adaquately describing the flow. Most investigators had difficulty in detecting the variations in pressure which occured in the short radial distances, since the entire process of acceleration and shock interaction may take place in a radial distance of only a few thousandths of an inch in a film thickness which is

less than a thousandth of an inch. Pressure measurements attempted with fixed pressure taps of significant hole size can quite easily miss the whole shock interaction area.

Thus, because of the lack of experimental data in this flow regime, the present investigation was undertaken.

2. Description of Experimental Equipment.

This investigation was conducted in two parts; first the determination of the pressure distribution of air in radial flow in thin films was done at the International Business Machines Research Laboratory in San Jose, California, and second, the determination of the mass rate of flow was done at the United States Naval Postgraduate School in Monterey, California.

The experimental equipment used at IBM Research Laboratory consisted of a device for holding a circular flat plate with a centrally located air supply hole above another flat plate which contained a two-mil pressure sensing hole. This device is shown schematically in Figure 1.

Two different upper plates were used. These plates had the same outside diameters but different air supply hole diameters. For the purpose of identification the upper plate with the smaller air supply hole diameter (.0218 inches) will be designated the "A" head, and the upper plate with the larger air supply hole diameter (.0343 inches) will be designated the "B" head throughout this investigation.

The diameters of the air holes were determined by measurements made with a traveling microscope. These diameters were verified by photomicrographs taken with a diffraction grating lying over the air hole. These photomicrographs also showed that the holes in the upper plates were round. The outside diameter of both upper plates A and B were measured with micrometer calipers. The flatness of both the upper and lower plates was determined by measurements made by optical flats using a monochromatic light source. The values determined by these measurements are shown in Table I.

The upper plate was mounted in a gimbal ring supported by a pivoted loading arm such that the centerline of the air supply hole of the upper plate was accurately located at a distance of three inches from the pivot point.

Loads were applied to the upper plate by adding known weights to the loading arm at a knife-edged support accurately located at a distance of nine inches from the pivot point and on the same side as the upper plate.

The weight of the loading arm, gimbal ring, and upper plate were counter balanced by a movable counterweight located on the opposite side of the

pivot point from the upper plate.

Use of the pivoted loading arm and gimbal ring permitted the upper plate freedom to translate vertically and to rotate about any axis parallel to the lower plate.

Both the loading arm and the gimbal were equpped with miniature precision ball bearings at their pivot points.

The lower plate containing a two-mil pressure sensing hole, was power driven by a screw operated through a variable speed transmission and electric motor. The lower plate was moved by the power drive in a direction parallel to the loading arm. At right angles to the power driven screw was a manually operated screw which would drive the plate in a direction normal to the loading arm. By using these screws in combination, it was possible to pick out any desired radial location under the upper plate. Both screws had precision ground threads and were equipped with micrometer dials.

The lower plate was equipped with precision linear potentiometers which were supplied by a regulated direct current power supply. Through the use of one of these potentiometers, an electrical signal indicating the radial position of the pressure sensing hole was sent to the X axis of a Mosely X-Y plotter.

The two-mil pressure sensing hole in the lower plate was connected to a Consolidated Electrodynamics Corporation Model 4-313 pressure transducer which employs a four arm strain gage bridge. An alternating current signal was supplied to the gage bridge by a Tektronix "Q" unit. Resulting pressure signals from the gage bridge were converted to direct current signals by the Tektronix "Q" unit and fed to the input of a Tektronix Oscilloscope. These signals were amplified in the Tektronix Oscilloscope and were sent from the vertical deflection plates of this oscilloscope, through a cathode follower, to the Y axis of the X-Y plotter.

In this way, it was possible to get continuous traces on the X-Y plotter which represented radial location of the pressure sensing hole versus pressure.

Stagnation pressure at the inlet to the supply hole of the upper plate was measured by a precision pressure gage manufactured by Wallace and Tierman Company.

Two precision pressure regulators connected in series were used to accomplish pressure regulation from a filtered 150 PSIG supply.

The experimental equipment used at the United States Naval Postgraduate School in the determination

of film thickness and mass rate of flow consisted of a test device which was essentially the same as that used at the IBM Research Laboratory. The upper plates and gimbal ring used in this phase of the experiment were the same units that were used at IBM. This gimbal ring and the two upper plates that were used in the investigation are shown in Figure 2. Figure 3 is a photograph of the test device used at the Postgraduate School.

The lower plate on this device did not contain a pressure sensing hole and the lower plate was not traversed. The lower plate contained two brackets, each of which supported one end of a Tuckerman optical strain gage oriented in a vertical plane.

The other end of the Tuckerman optical strain gage was secured to the upper plate loading arm at points located exactly the same distance from the loading arm pivot as the upper plate supply hole center line. Two Tuckerman Autocollimators were used with these gages to determine film thickness.

The mass rate of flow of air between the parallel plates was determined by the use of a calibrated Flowrator manufactured by the Fischer and Porter Co.

Stagnation pressure of the air at the entrance to the supply hole in the upper plate was measured

by a precision pressure gage manufactured by the Ashcroft Company.

Stagnation temperature at the inlet was determined by a copper-constantan thermocouple and a Leeds and Northrup Potentiometer.

Pressure regulation of the filtered 100 PSIG supply was accomplished by the use of a pressure reducer and throttling valve.

3. Experimental Procedure

Part I. Pressure Distribution Investigation

With the desired upper plate accurately located in the loading arm, the experimental procedure was as follows:

With the upper and lower plates fixed in direct contact such that the air supply hole in the upper plate was directly over the pressure sensing hole in the lower plate, the pressure transducer was calibrated. The Wallace and Tierman precision gage was used to calibrate the pressure transducer. At this time the sensitivity of the Y axis of the X-Y plotter was adjusted so that the maximum stagnation pressure employed produced full scale deflection. The upper plate was then released and allowed to float on a film of air while the linear potentiometer indicating radial location was calibrated and the X axis sensitivity of the X-Y recorder was adjusted for a suitable deflection over the diameter of the upper plate.

The air supply through the upper plate was then shut off and the loading arm was balanced. The desired load was then applied to the loading arm by weight in a scale pan with knife edge supports to the loading arm.

Pressure was again supplied to the hole in the upper plate. This pressure was adjusted until the upper plate was floating freely on a film of air. The location of the pressure sensing hole was next determined by use of power driven and manually driven screws to move the lower plate. The location of the rapid pressure drop delineating the edge of the hole was determined in two directions perpendicular to each other. By use of the micrometer dials attached to these two screws, it was possible to determine the location of the center of the supply hole of the upper plate with respect to the center of the pressure sensing hole.

The pressure sensing hole in the lower plate was then moved to a location at the edge of the upper plate. The motor drive was turned on driving the pressure sensing hole slowly across the diameter of the upper plate. The lowest speed available using power drive of the lower plate was approximately 1/2 inch per hour. This speed was used in the region where rapid pressure changes were anticipated. In the lower pressure regions the speed of the power drive was increased above 1/2 inch per hour so that excessive time would not be consumed and so that "drift" of the electronic components would not be a

problem. The time required to traverse the diameter of the upper plate was approximately one-half hour. Both the calibration of the pressure transducer and the linear potentiometer indicating radial displacement were checked at the beginning and end of each run. A run consisted of a single pressure traverse at one fixed stagnation pressure and one upper plate loading.

Parallelism of the upper and lower plates was checked by making a series of traverses with the power driven screw at various offsets obtained by adjusting the manual driven screw located at right angles to the power driven screw. Correspondence of pressure profiles along two mutually perpendicular diameters of the upper plate was assumed to prove that the upper and lower plates were parallel.

The oscilloscope, pressure transducer, and other electrical auxiliaries were allowed to warm up for at least one hour before use. Warm up was continued until these units stabilized.

Because of the extremely small vertical displacements of the upper plate or film thicknesses and to employ the maximum capability provided by the flatness of the surfaces it was necessary that both the upper and lower plates be cleaned with acetone and optical wiping papers before assembly.

Part II. Film thickness and mass rate of flow investigations.

The device used in these investigations was essentially the same as that used in the investigations of pressure distributions. The difference was that the lower plate did not contain a pressure sensing hole and was fixed.

The same upper plates and gimbal assembly as used in the pressure distribution determinations were used in the mass rate of flow and film thickness measurements. Assembly of this device was the same as that used in the pressure distribution investigations.

The Tuckerman optical strain gages used in determining the film thickness were applied to the bracket and loading arm after the upper plate had been assembled in the loading arm. The application of these gages is shown in Figure 3.

The loading arm was then balanced with the Tuckerman strain gages in position without disturbing the optical strain gage attachment.

The desired force was then applied to the upper plate by adding weights to the scale pan. The position assumed by the upper plate when these weights were on the scale pan and when no air was supplied to the upper plate was assumed to be the

position corresponding to zero film thickness. When this had been determined, air pressure was supplied to the upper plate while one of the Tuckerman optical strain gages was observed through the autocollimator. Pressure was increased slowly until the upper plate was floating on a film of air. The pressure was then slowly decreased until the film collapsed and the zero position of the Tuckerman optical strain gages was verified.

When these gages could be made to return to the same zero position, the determination of film thickness and mass rate of flow for a fixed load applied to the upper plate and variable stagnation pressure was started. The stagnation pressure was increased by increments as shown in the tabulation of experimental data, Table 2, to a maximum of approximately 90 PSIG. After the maximum pressure for a particular run was reached, the pressure was decreased by increments equal to those used while increasing the pressure. The readings of the Flowrator and each of the Tuckerman optical strain gages were recorded for each increment. If the film thicknesses and mass rate of flow for both an increment taken at increasing pressures and an increment taken at decreasing pressures were the same and the Tuckerman optical

strain gages returned to their original zero position, the run was considered to be satisfactory.

The stagnation temperature for each run was observed by the use of a copper-constantan thermocouple and a Leeds and Northrup potentiometer. Ambient temperature and pressure were noted for each run.

A calibration of the Flowrator used in the mass rate determination was made over the flow range and pressure range of the investigation. Calibration was accomplished by the use of two wet test meters with capacities of 10 cubic feet per hour and 150 cubic feet per hour. Appendix I contains the Flowrator Calibration Curve, Figure 27.

The Ashcroft pressure gage that was used in this investigation was calibrated with a dead weight tester.

4. Discussion of Results and Conclusions:

The data collected in the investigation of pressure distribution are presented as non-dimensional plots in Figures 4 through 19 and in tabular form in Table II.

Several plots, obtained on the X-Y plotter, which are representative of the raw data taken in the pressure distribution investigation are reproduced in Figures 20 through 22.

The data taken in the investigation of film thickness and mass rate of flow are presented in tabular form in Table III. Figures 23 and 24 are absolute plots of film thickness versus supply pressure and Figures 25 and 26 are plots of the observed mass rate of flow versus the theoretic maximum based on one dimensional adiabatic flow assuming choked flow through the cylindrical area defined by the film thickness and the diameter of the air supply hole in the upper plate.

An examination of the radial pressure distributions shows that sonic velocities in the cylindrical control area followed by expansion into the supersonic regime occured in some of the cases where the overall pressure ratio of $\frac{P_a}{P_o} < .528$ (required for

sonic velocity in a one dimensional reversible adiabatic expansion) existed. In other cases, sonic velocity was not reached and the pressure decreased gradually in viscous flow.

The investigation of film thickness and mass rate of flow shows that in the supersonic regime where $P/P_o \leq .528$, the actual mass rate of flow is predicted to within three per cent by Fleigner's Formula [8]:

$$\dot{m} = .532 \frac{P_o A}{\sqrt{T_o}}$$

where

P_o = stagnation pressure (PSIA)

T_o = stagnation temperature (^oR)

$A = \pi d_o h$ (in^2) (cylindrical control area)

$\dot{m}$ = mass rate of flow (lb_m/sec)

This regime corresponds to mass flow rates above 50×10^{-6} lb_m/sec. for the A head and mass flow rates above 80×10^{-6} lb_m/sec. for the B head as seen in Figures 25 and 26. Below these minimum flow rates sonic velocity did not occur either because $P_a/P_o > .528$ or because the viscous effects near the air supply hole prevented the gas from reaching sonic velocity. It was also noted that for the high rates of flow the observed mass rate of flow was lower than that predicted by theory, this was more evident in the tests ("A" runs) where the air supply hole was small.

This is explained by a consideration of how the stagnation pressure was measured, here we are seeing the effect of stagnation pressure loss between the pressure gage and the air supply hole exit. This is also evident in the pressure profiles, since complete pressure recovery was not obtained when the pressure sensing hole was located directly beneath the air supply hole in the upper plate.

Further examination of the pressure profiles shows that for the smaller diameter air supply hole and a heavy load, the entire process of sonic flow, at the edge of the air supply hole, followed by expansion into the supersonic flow regime, shock and pressure recovery, occured over a very small radial distance (.0269 inches from sonic velocity to pressure recovery in Run No. 1-A, Figure 11) and that in this region of heavy load and thin films the shock approximated the thin normal shock that is experienced in supersonic nozzle diffusers.

As the load on the upper plate was decreased, the film thickness increased, the area covered by supersonic flow was enlarged, see Figure 13 for example, local pressures became subambient, and the shock became a distributed shock similar in nature to that which occurs in pipe flow. (Discussed by Shapiro [8] pp 135-137).

An examination of the plots of film thickness versus supply pressure, (Figures 23 and 24), shows that the upper plate functions much more efficiently in terms of air consumption, as a load supporting device when the supply pressure is reduced. It can be seen, for example, that for the "A" head we can support a load of 600 grams with a supply pressure of 70 PSIG and a film thickness of approximately 1-mil or we can support the same load with a supply pressure of 30 PSIG and a film thickness of about .72 mil. Recalling that the air flow rate is approximated by $\dot{m} = C_1 P_s h$ for a fixed stagnation temperature and supply hole diameter, it is easily concluded that the most efficient area of operation for an air lubricated pad bearing is in the region of viscous films. However, if we consider that our bearing may be required to operate in the presence of accelerations that may be continued for some time, (inertial guidance systems in rockets for example), we must consider what would happen if this bearing were subjected to an increased load for an extended period. An examination of the plot of Film Thickness versus Supply Pressure For The "A" Pad shows that a load of 900 grams could not be supported with a 30 PSIG supply pressure. However,

if the supply pressure were 70 PSIG and the force were increased to 900 grams the clearance (h) would be reduced to approximately.78 mils.

Gross [5] has stated that the gas compressibility at the entrance supply section may tend to cause pneumatic instability resulting in plate vibration. He suggests that the air supply hole volume be reduced. This of course must be done at a sacrifice of load carrying capacity as is indicated by a comparison of the film thickness - pressure characterists of pads A and B in the plots of film thickness versus Gage Pressure, Figures 23 and 24.

5. Recommendations for further work.

It appears that further work could be done in two areas; an investigation of geometry factors and an investigation of the temperature distribution of air in radial flow.

An investigation of geometry factors should be concerned with the influence of variations of both absolute and relative geometric factors. A parameter such as r_o/R_1 (where r_o is the radius of the air supply hole and R_1 is the outer radius of the pad), might be chosen and an investigation made with this parameter a constant and the absolute values r_o and R_1 variable, then perhaps R_1 could be selected as a variable with r_o constant. Such an investigation would yield data which should enable the correlation of film thickness, loading, mass rate of flow, and stagnation pressure in a non-dimensional form.

In the analysis of the gas dynamics of the radial flow, two limiting cases have been proposed. The viscous flow regime has suggested isothermal flow as the limit most nearly approached, whereas the supersonic regime suggests adiabatic flow analysis. It may be of interest, therefore, to investigate the actual radial temperature distribution.

Bibliography

(1) "Sur les Principaux Phenomenes Qui Presentent les Frottements Mediats", by G. Hirn, Bulletin de la Societe Industrielle de Mulhouse, Vol. 26, 1854 p. 188 (French)

(2) "Experiments with an Air Lubricated Journal Bearing", by A. Kingsbury, ASME Journal, Vol. 9, 1897, pp 267-292

(3) "Theory and Practice of Lubrication for Engineers", by D.D. Fuller, John Wiley and Sons, Inc., N.Y., N.Y. 1956, p 287

(4) "Hydrostatic Gas Bearings", by J.H. Laub, Journal of Basic Engineering Transactions of the ASME Series D, June 1960

(5) "Film Lubrication IX, Externally Pressurized Bearings", by W.A. Gross, International Business Machines Technical Report, RJ117-9, 1960

(6) "Ecoulement D'Un Fluide Entre Deux Plans Paralleles Contribution A L'Etude Des Butees D'Air", by R. Comolet, Publications Scientifiques et Techniques No. 344, 1957 (French)

(7) "A Theoretical Investigation of Pressure Depression in Externally Pressurized Gas-Lubricated Circular Thrust Bearings", by H. Mori, Paper No. 60-Lub 6, The American Society of Mechanical Engineers

(8) "Compressible Fluid Flow", by A.H. Shapiro, Vol. 1, The Ronald Press Co., N.Y., N.Y. 1953

Table I

PHYSICAL MEASUREMENTS OF UPPER AND LOWER PLATES

	Lower Plate	Upper Plates A	B
OUTSIDE DIAMETER (in.)	---	0.6610	0.6610
AIR HOLE DIAMETER (in.)	0.002	0.0218	0.0343
FLAT TO WITHIN - (λ in.)	9*	6	6
SURFACE ROUGHNESS (μ in. RMS)	3	4	4

*Taken over a 3 inch diameter circular portion centered on the pressure sensing hole.

Table II

Run 1-A		Run 2-A	
F = 600 gm.	P_o = 44.6PSIA	F = 600 gm.	P_o = 54.6PSIA
T_o = 76°F	P_a = 14.6PSIA	T_o = 74°F	P_a = 14.6PSIA
r/R	$\frac{P-P_a}{P_o}$	r/R	$\frac{P-P_a}{P_o}$
0	.600	0	.712
.030	.600	.034	.274
.035	.224	.035	.183
.036	.499	.035	.0914
.041	.0695	.035	.0713
.042	.112	.035	.208
.060	.170	.039	.0366
.117	.220	.039	.141
.200	.195	.045	.0147
.298	.170	.053	.0366
.487	.112	.062	.0914
.716	.056	.105	.208
.850	.0336	.126	.221
.891	.0224	.175	.208
1.00	0	.241	.183
		.379	.141
		.502	.0713
		.795	.0366
		1.00	0

Table II (Cont.)

Run 3-A		Run 4-A	
F = 600 gm.	P_o = 74.6PSIA	F = 600 gm.	P_o = 94.6PSIA
T_o = 75°F	P_a = 14.6PSIA	T_o = 76°F	P_a = 14.6PSIA

r/R	$\frac{P-P_a}{P_o}$	r/R	$\frac{P-P_a}{P_o}$
0	.693	0	.786
.021	.693	.027	.740
.030	.670	.030	.634
.031	.535	.036	.528
.031	.402	.037	.422
.033	.268	.037	.317
.035	.134	.037	.211
.036	.067	.037	.159
.041	.0334	.037	.106
.045	.0134	.042	.0528
.054	0	.043	.0243
.063	-.0054	.048	.0106
.079	0	.063	0
.085	.0134	.087	-.0106
.090	.0255	.111	0
.099	.0334	.122	.0106
.126	.067	.133	.0243
.136	.0911	.157	.0528
.146	.0958	.164	.0703
.163	.0857	.172	.0745
.199	.0911	.208	.0702
.300	.0737	.310	.0634
.400	.067	.457	.0528
.581	.0482	.596	.0370
.825	.0255	.729	.0243
.879	.0134	.874	.0106
1.00	0	1.00	0

Table II (Cont.)

Run 5-A		Run 6-A	
F = 600 gm.	P_o = 114.6PSIA	F = 300 gm.	P_o = 44.6PSIA
T_o = 75°F	P_a = 14.6PSIA	T_o = 76°F	P_a = 14.6PSIA
r/R	$\frac{P-P_a}{P_o}$	r/R	$\frac{P-P_a}{P_o}$
0.00	.866	.0181	.651
.0271	.785	.0305	.560
.030	.699	.031	.392
.030	.611	.031	.280
.033	.436	.032	.202
.033	.349	.035	.168
.036	.0874	.036	.0824
.037	.0655	.037	.0448
.039	.0436	.038	.0157
.039	.0175	.039	0.00
.040	.0175	.042	-.0190
.048	.0096	.048	-.0224
.057	0.00	.053	-.0190
.069	-.0074	.066	0.00
.090	-.0166	.069	.0157
.099	-.0262	.074	.0291
.133	-.0349	.081	.0448
.157	-.0262	.102	.0875
.175	-.0175	.108	.119
.190	-.0078	.115	.112
.199	0.00	.128	.128
.205	.0096	.199	.119
.211	.0175	.253	.112
.218	.0436	.394	.0875
.229	.0501	.488	.0695
.238	.0524	.656	.0449
.262	.0502	.775	.0291
.325	.0450	.885	.0157
.421	.0437	1.00	0.00
.542	.0297		
.686	.0175		
.850	.0096		
1.00	0.00		

Table II (Cont.)

Run 7-A		Run 8-A	
F = 300 gm.	P_o = 54.6PSIA	F = 300 gm.	P_o = 74.6PSIA
T_o = 76°F	P_a = 14.6 PSIA	T_o = 76°F	P_a = 14.6PSIA
r/R	$\frac{P-P_a}{P_o}$	r/R	$\frac{P-P_a}{P_o}$
0.00	.694	0.00	.732
.027	.641	.030	.670
.030	.549	.036	.335
.030	.457	.037	.201
.031	.320	.0377	.169
.033	.274	.037	.1325
.036	.185	.037	.0682
.037	.0915	.038	.0535
.039	.0586	.042	.0335
.042	.032	.043	.0149
.042	.0183	.045	.0074
.042	0.00	.054	0.00
.048		.060	-.0127
.054	-.0210	.066	-.0214
.060	-.0274	.074	-.0301
.069	-.0210	.090	-.0365
.084	-.0146	.107	-.0301
.090	0.00	.121	-.0214
.111	.0183	.130	-.0128
.114	.032	.145	0.00
.120	.0585	.148	.0074
.130	.0915	.150	.0148
.141	.0951	.157	.0335
.199	.0975	.163	.0535
.332	.0732	.175	.0629
.458	.0585	.211	.0582
.554	.0439	.289	.0535
.579	.042	.398	.0442
.686	.032	.536	.0335
.814	.0183	.686	.0268
1.00	0.00	.765	.0147
		.885	.0736
		1.00	0.00

Table II (Cont.)

Run 9-A		Run 10-A	
F = 300 gm.	P_o = 94.6 PSIA	F = 900 gm.	P_o = 94.6PSIA
T_o = 76°F	P_a = 14.6 PSIA	T_o = 78°F	P_a = 14.6PSIA
r/R	$\frac{P-P_a}{P_o}$	r/R	$\frac{P-P_a}{P_o}$
0.00	.819	0.00	.830
.027	.740	.030	.740
.030	.634	.031	.634
.030	.529	.033	.528
.033	.422	.035	.422
.036	.317	.036	.374
.036	.211	.036	.317
.037	.106	.037	.211
.037	.0792	.040	.185
.037	.0529	.043	.106
.048	.0264	.046	.0782
.054	0.00	.050	.0528
.060	-.019	.055	.0264
.102	-.0676	.066	0.00
.127	-.0423	.078	.0264
.160	-.0190	.090	.0528
.175	0.00	.096	.155
.187	.0264	.114	.158
.208	.0529	.121	.182
.344	.0422	.196	.158
.521	.0264	.307	.128
.765	.0106	.394	.106
1.00	0.00	.536	.0792
		.68	.0528
		1.00	0.00

Table II (Cont.)

Run 11-A		Run 12-A	
F = 900 gm.	P_o = 74.6PSIA	F = 900 gm.	P_o = 54.6PSIA
T_o = 78°F	P_a = 14.6PSIA	T_o = 78°F	P_a = 14.6PSIA

r/R	$\frac{P-P_a}{P_o}$	r/R	$\frac{P-P_a}{P_o}$
0.00	.796	0.00	.715
.033	.670	.035	.549
.036	.536	.037	.457
.037	.402	.038	.366
.037	.268	.043	.274
.037	.201	.046	.209
.037	.134	.055	.274
.042	.101	.067	.308
.046	.0670	.101	.358
.049	.0536	.183	.308
.054	.0455	.244	.274
.056	.0535	.427	.183
.060	.067	.585	.137
.066	.101	.707	.0915
.078	.134	.841	.0457
.101	.201	1.00	0.00
.136	.237		
.229	.201		
.403	.134		
.548	.101		
.669	.067		
.729	.0536		
.850	.0268		
1.00	0.00		

Table II(Cont.)

Run 13-A F = 900 gm. P_o = 46.6PSIA T_o = 78°F P_a = 14.6PSIA		Run 1-B F = 600 gm. P_o = 94.6PSIA T_o = 76°F P_a = 14.6PSIA	
r/R	$\frac{P-P_a}{P_o}$	r/R	$\frac{P-P_a}{P_o}$
0.00	.686	0.00	.810
.037	.644	.049	.74
.043	.465	.051	.634
.064	.470	.052	.529
.116	.430	.052	.423
.244	.322	.055	.317
.420	.213	.058	.264
.579	.161	.059	.211
.690	.1075	.059	.159
1.00	0.00	.061	.106
		.071	.0792
		.079	.0529
		.085	.0264
		.095	0.00
		.135	-.042
		.172	0.00
		.197	.0264
		.219	.0529
		.231	.0892
		.250	.106
		.380	.0872
		.590	.0529
		.740	.0264
		1.00	0.00

Table II (Cont.)

Run 2-B		Run 3-B	
F = 600 gm.	P_o = 74.6PSIA	F = 600 gm.	P_o = 54.6PSIA
T_o = 76°F	P_a = 14.6PSIA	T_o = 76°F	P_a = 14.6PSIA
r/R	$\frac{P-P_a}{P_o}$	r/R	$\frac{P-P_a}{P_a}$
0.00	.775	0.00	.720
.035	.775	.030	.720
.050	.737	.050	.672
.050	.670	.054	.549
.051	.560	.058	.457
.052	.469	.059	.366
.054	.402	.059	.274
.058	.335	.059	.183
.058	.268	.060	.137
.059	.201	.062	.0915
.059	.134	.065	.0458
.059	.101	.072	.0183
.062	.101	.075	.0147
.070	.067	.078	.0183
.079	.0335	.088	.0457
.090	0.00	.100	.0915
.098	-.0134	.120	.137
.108	-.0268	.149	.183
.115	-.0134	.190	.252
.121	0.00	.300	.183
.140	.0335	.580	.137
.160	.067	.620	.0915
.181	.101	.800	.0457
.195	.134	.920	.0183
.210	.147	1.00	0.00
.278	.134		
.450	.101		
.600	.067		
.800	.0335		
1.00	0.00		

Table II (Cont.)

Run 4-B				Run 5-B			
F	600 gm.	P_o	44.6PSIA	F	600 gm.	P_o	34.6PSIA
T_o	77°F	P_a	14.6PSIA	T_o	78°F	P_a	14.6PSIA

r/R	$\frac{P-P_a}{P_o}$	r/R	$\frac{P-P_a}{P_o}$
0.00	.671	0.00	.578
.038	.671	.047	.578
.051	.561	.050	.537
.054	.449	.055	.489
.056	.336	.058	.433
.058	.224	.060	.416
.058	.168	.092	.416
.059	.112	.100	.410
.060	.0784	.252	.289
.070	.112	.388	.217
.084	.168	.550	.145
.112	.224	.759	.072
.160	.246	1.00	0.00
.290	.224		
.460	.168		
.600	.112		
.795	.056		
.900	.224		
1.00	0.00		

Table II (Cont.)

Run 6-B		Run 7-B	
F = 300 gm.	P_o = 94.6PSIA	F = 300 gm.	P_o = 74.6PSIA
T_o = 78°F	P_a = 14.6PSIA	T_o = 78°F	P_a = 14.6PSIA
r/R	$\frac{P-P_a}{P_a}$	r/R	$\frac{P-P_a}{P_a}$
0.00	.846	0.00	.771
.030	.846	.028	.771
.040	.80	.044	.737
.050	.74	.051	.670
.054	.634	.055	.536
.056	.529	.055	.402
.057	.423	.055	.268
.058	.317	.055	.201
.058	.264	.057	.1341
.058	.211	.057	.0107
.058	.159	.058	.0804
.059	.106	.062	.0670
.070	.0794	.068	.0335
.072	.0529	.076	0.00
.078	.0264	.079	-.0134
.088	0.00	.085	-.0335
.099	-.0264	.096	-.0536
.120	-.0529	.107	-.0670
.160	-.0655	.117	-.0737
.190	-.0529	.129	-.0831
.219	-.0264	.138	-.0737
.255	0.00	.154	-.0536
.265	.0264	.171	-.0335
.275	.0529	.192	-.0134
.290	.0655	.207	0.00
.362	.0529	.215	.0134
.689	.0264	.225	.0335
1.00	0.00	.232	.0536
		.236	.0670
		.239	.0737
		.279	.0737
		.321	.0670
		.438	.0536
		.610	.0335
		.722	.0268
		.885	.0074
		.994	.0134
		1.00	0.00

Table II (cont.)

Run 8-B		Run 9-B	
F = 300 gm. P_o = 54.6PSIA		F = 300 gm. P_o = 44.6PSIA	
T_o = 78°F P_a = 14.6PSIA		T_o = 79°F P_a = 14.6PSIA	
r/R	$\frac{P-P_a}{P_a}$	r/R	$\frac{P-P_a}{P_a}$
0.00	.696	0.00	.639
.032	.700	.040	.639
.040	.691	.048	.617
.047	.641	.050	.561
.051	.550	.054	.337
.054	.366	.055	.1122
.054	.1832	.055	.0551
.055	.0916	.057	.0224
.057	.0550	.058	0.00
.060	.0183	.059	-.0224
.065	0.00	.062	-.0449
.067	-.0183	.064	-.0551
.075	-.0458	.070	-.0897
.081	-.0733	.077	-.1055
.088	-.0916	.087	-.0897
.090	-.0971	.093	-.0551
.097	-.1047	.106	-.0224
.107	-.0916	.118	0.00
.122	-.0550	.131	.0224
.134	-.0366	.145	.0449
.181	.0366	.151	.0551
.193	.0733	.173	.0897
.198	.0824	.182	.1010
.214	.0897	.193	.1122
.325	.0550	.214	.1101
.600	.0366	.314	.0897
.757	.0182	.518	.0551
1.00	0.00	.670	.0336
		.771	.0224
		1.00	0.00

Table II (Cont.)

Run 10-B		Run 11-B	
F = 300 gm. P_o = 34.6PSIA		F = 300 gm. P_o = 24.6PSIA	
T_o = 79°F P_a = 14.6PSIA		T_o = 79°F P_a = 14.6PSIA	
r/R	$\frac{P-P_a}{P_o}$	r/R	$\frac{P-P_a}{P_o}$
0.00	.541	0.00	.423
.030	.541	.023	.423
.043	.520	.051	.423
.045	.506	.055	.394
.049	.434	.086	.368
.052	.289	.144	.305
.054	.144	.282	.203
.056	0.00	.558	.1016
.057	-.0289	.786	.0407
.058	-.0607		
.070	-.0289		
.088	.0289		
.089	.0462		
.100	.0636		
.128	.1157		
.136	.130		
.165	.1444		
.208	.1502		
.242	.144		
.438	.0867		
.643	.0578		
.767	.0289		
1.00	0.00		

Table II (Cont.)

Run 12-B		Run 13-B	
F = 900 gm.	P_o = 94.6PSIA	F = 900 gm.	P_o = 74.6PSIA
T_o = 76°F	P_a = 14.6PSIA	T_o = 76°F	P_a = 14.6 PSIA
r/R	$\frac{P-P_a}{P_a}$	r/R	$\frac{P-P_a}{P_o}$
0.00	.872	0.00	.791
.028	.873	.019	.791
.042	.867	.032	.784
.045	.856	.043	.777
.048	.846	.048	.737
.050	.825	.053	.536
.052	.740	.056	.161
.054	.423	.058	.134
.058	.2115	.064	.107
.062	.1640	.069	.0806
.069	.1058	.074	.0670
.076	.0793	.076	.0469
.082	.0529	.083	.0429
.088	.0423	.086	.0375
.093	.0264	.089	.0402
.100	.0212	.135	.134
.110	.0190	.181	.201
.113	.0212	.191	.208
.121	.0317	.199	.211
.141	.0634	.212	.208
.187	.1268	.291	.174
.200	.1586	.940	.0134
.208	.1745	1.00	0.00
.219	.1788		
.234	.1745		
.266	.1640		
.319	.1480		
.643	.0793		
.755	.0529		
.901	.0106		
1.00	0.00		

Table II (Cont.)

Run 14-B		Run 15-B	
F = 900 gm.	P_o = 54.6PSIA	F = 900 gm.	P_o = 54.6PSIA
T_o = 78°F	P_a = 14.6PSIA	T_o = 78°F	P_a = 14.6PSIA

r/R	$\frac{P-P_a}{P_o}$	r/R	$\frac{P-P_a}{P_o}$
0.00	.732	0.00	.673
.051	.549	.044	.673
.052	.458	.052	.561
.052	.366	.055	.448
.053	.274	.061	.408
.054	.183	.079	.408
.059	.165	.100	.417
.070	.183	.122	.417
.085	.220	.158	.397
.098	.256	.242	.336
.110	.274	.305	.291
.157	.336	.421	.224
.225	.284	.557	.168
.290	.238	.682	.112
.335	.220	.836	.056
.429	.183	1.00	0.00
.561	.137		
.692	.0915		
.830	.0458		
1.00	0.00		

Table II (Cont.)

Run 16-B	
F = 900 gm.	P_o = 40.6PSIA
T_o = 78°F	P_a = 14.6PSIA
r/R	$\frac{P-P_a}{P_o}$
0.00	.640
.049	.640
.055	.616
.069	.554
.107	.492
.149	.431
.238	.370
.415	.246
.537	.185
.685	.123
.818	.062
1.00	0.00

Table III

Run	P_o PSIA	h mils	m_o #/sec.
A HEAD F = 300 gm.		Pa = 14.9 PSIA T_o = 536° R	
M1A	27.9	.650	22
M2A	28.4	.682	25
M3A	28.9	.734	30
M4A	29.4	.780	34
M5A	32.4	.894	47
M6A	34.9	.941	55
M7A	44.9	1.07	76
M8A	54.9	1.17	99
M9A	64.9	1.26	126
M10A	74.9	1.34	152
M11A	84.9	1.40	180
M12A	94.9	1.48	207
M13A	104.9	1.55	---
A HEAD F = 600 gm.		Pa = 14.9 T_o = 536	
M14A	34.7	.386	11
M15A	39.9	.605	35
M16A	42.2	.669	
M17A	44.9	.708	51
M18A	54.9	.789	69
M19A	64.9	.867	89
M20A	74.9	.927	109
M21A	84.9	.986	131
M22A	94.9	1.04	152
M23A	102.3	1.09	170

Table III (Cont.)

A HEAD
F = 900 gm.

Pa = 14.9 PSIA
T_o = 536° R

Run	P_o PSIA	h mils	m_o #/sec.
M24A	46.9	.421	23
M25A	47.9	.465	29
M26A	48.9	.512	35
M27A	49.9	.525	39
M28A	50.0	.539	40
M29A	50.4	.544	43
M30A	51.4	.567	46
M31A	54.9	.603	55
M32A	64.9	.667	71
M33A	74.9	.722	87
M34A	84.9	.770	105
M35A	94.9	.817	124
M36A	104.9	.861	145

B HEAD
F = 300 gm.

Pa= 14.9 PSIA
T_o= 537° R

Run	P_o PSIA	h mils	m #/sec.
M1B	27.5	.925	52
M2B	29.9	1.09	81
M3B	34.9	1.20	109
M4B	44.9	1.34	149
M5B	54.9	1.44	195
M6B	64.9	1.54	240
M7B	74.9	1.61	297
M8B	84.9	1.67	---
M9B	94.9	1.76	---

Table III (Cont.)

B HEAD
F = 600 gm.

P_a = 14.9 PSIA
T_o = 536° R

Run	P_o PSIA	h mils	m #/sec.
M10B	34.9	.459	16
M11B	37.4	.769	62
M12B	39.9	.845	83
M13B	44.9	.923	106
M14B	54.9	1.02	141
M15B	64.9	1.10	180
M16B	74.9	1.18	220
M17B	84.9	1.24	262
M18B	94.9	1.31	306
M19B	99.4	1.34	331

B HEAD
F = 900 gm.

P_a = 14.9 PSIA
T_o = 535° R

Run	P_o PSIA	h mils	m #/sec.
M20B	43.9	.542	38
M21B	44.9	.613	53
M22B	47.9	.704	78
M23B	49.9	.750	91
M24B	54.9	.802	112
M25B	64.9	.874	145
M26B	74.9	.940	176
M27B	84.9	.985	217
M28B	94.9	1.06	248

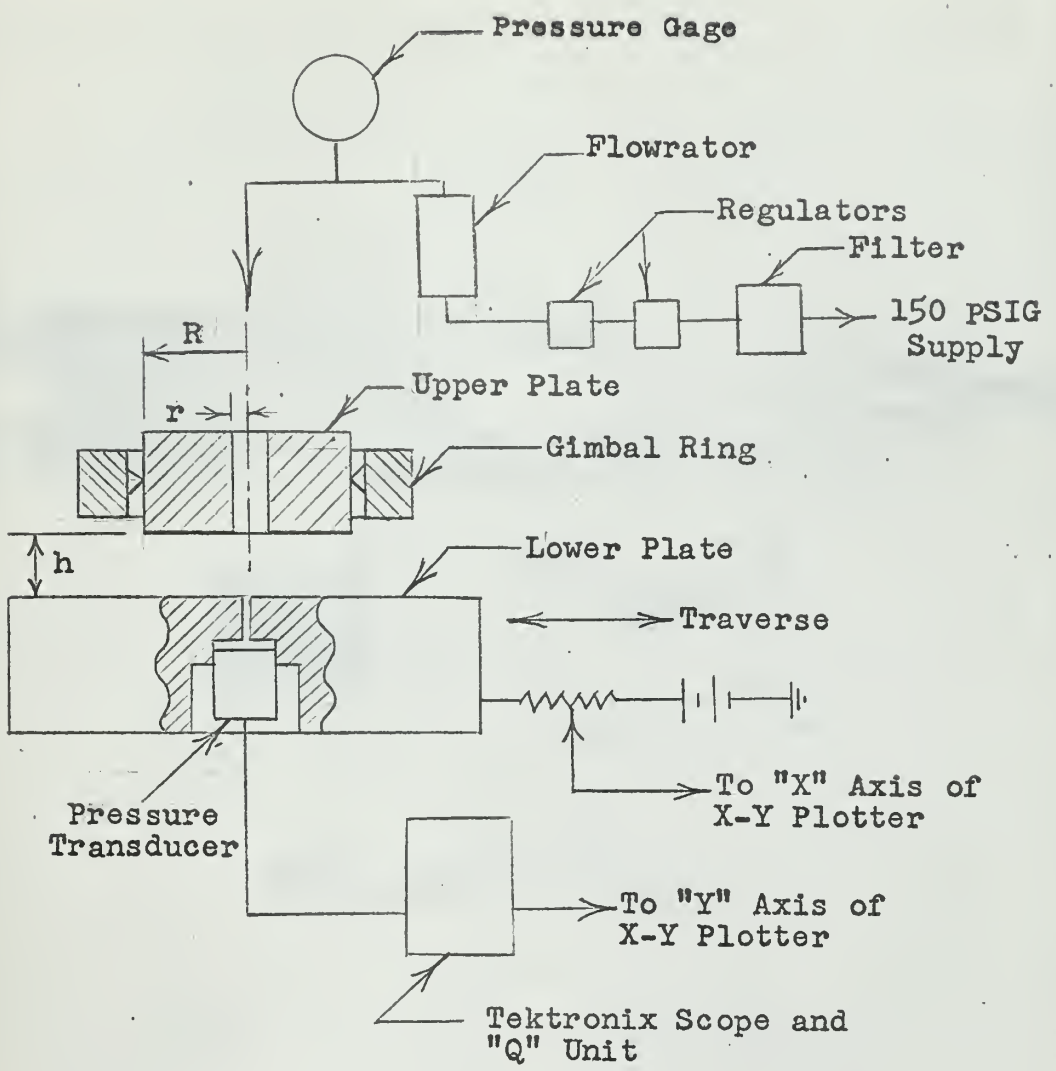

Fig. 1
Schematic of pad bearing
and test equipment used
in Pressure Distribution
Investigation

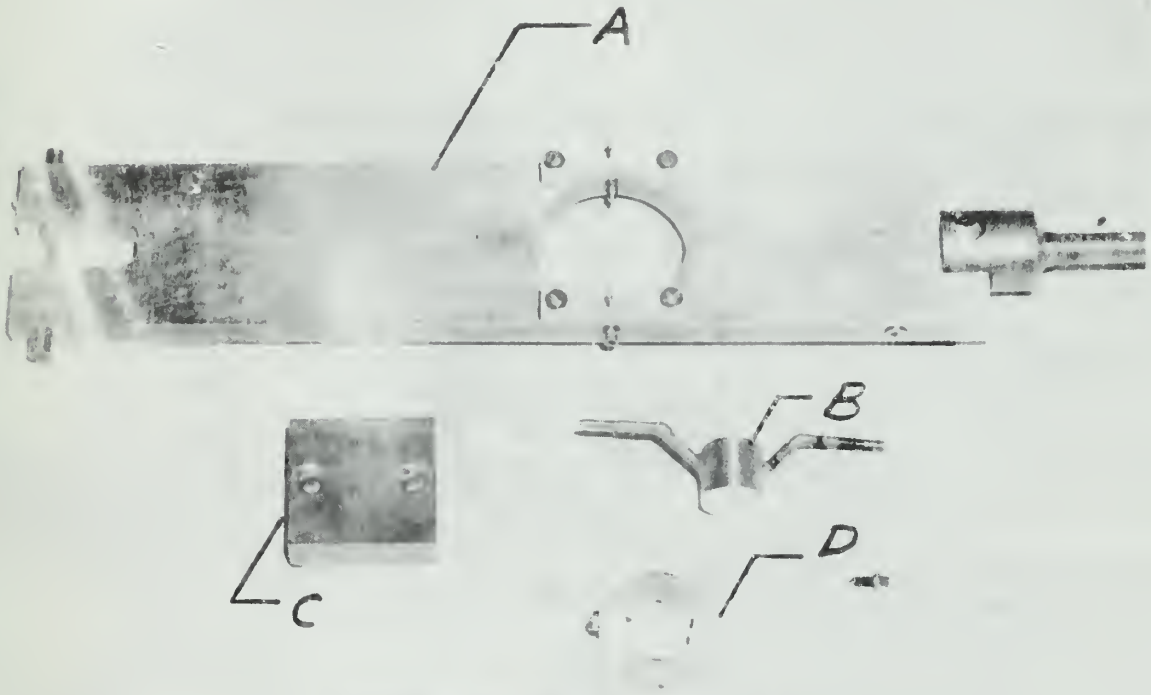

Figure 2

Photograph of Gimbal Ring and Air [illegible]

A - Loading Arm
B - Air Head
C - [illegible] Plate
D - [illegible] Ring

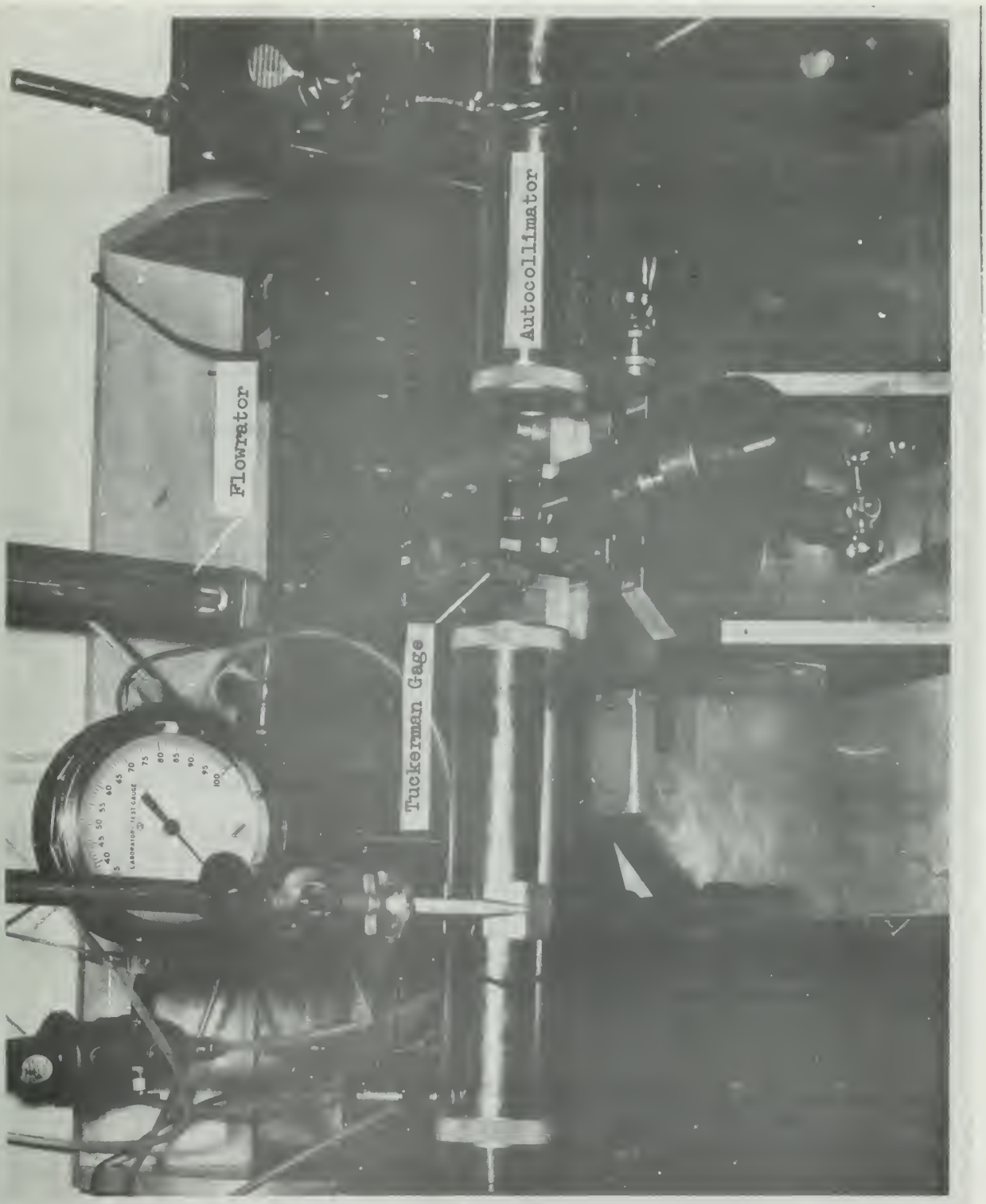

Figure 3

Photograph of Test Device used
in Film Thickness and Mass Rate
of Flow Investigation

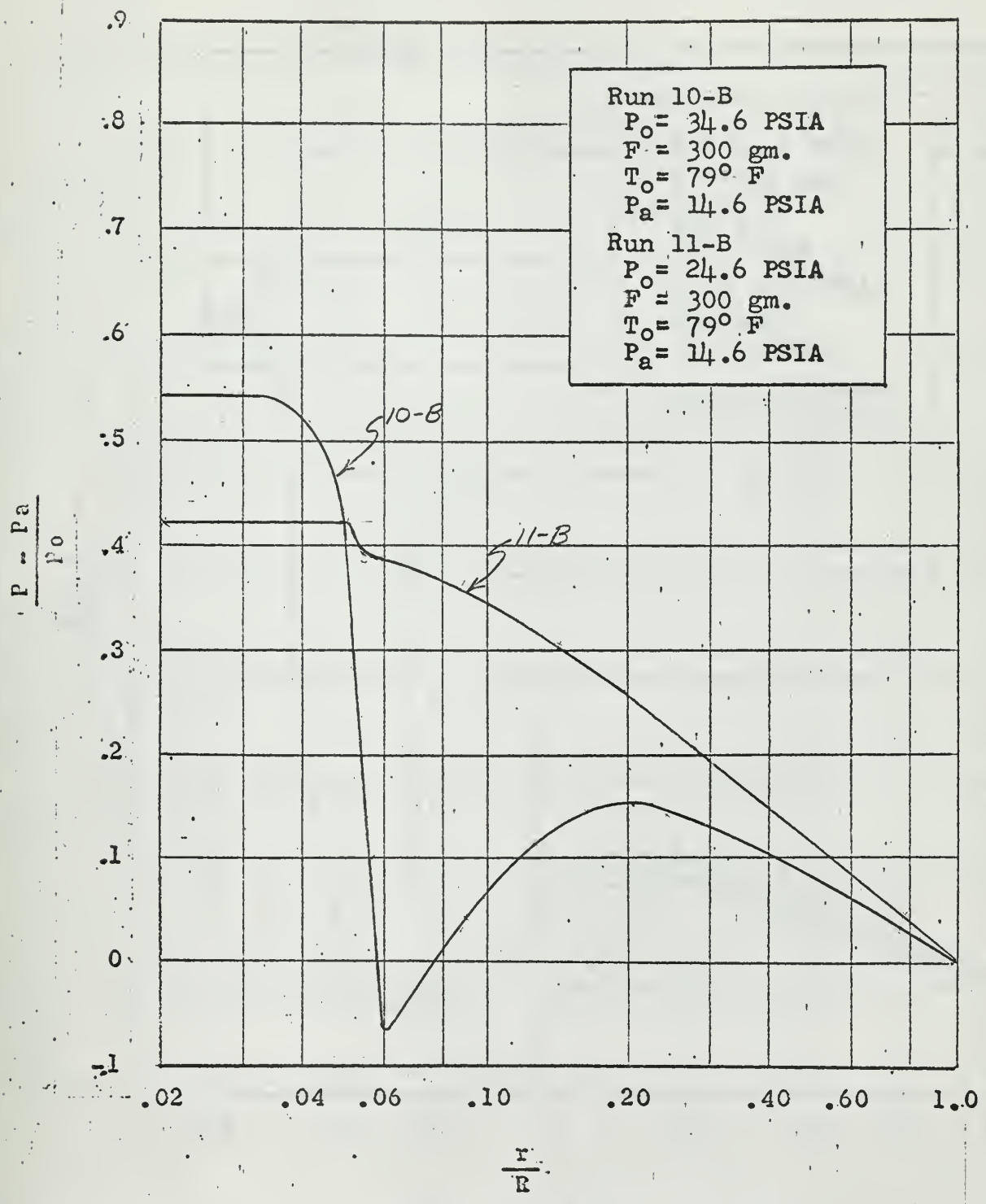

Fig. 4 - Plot of non-dimensional pressure versus radius ratio

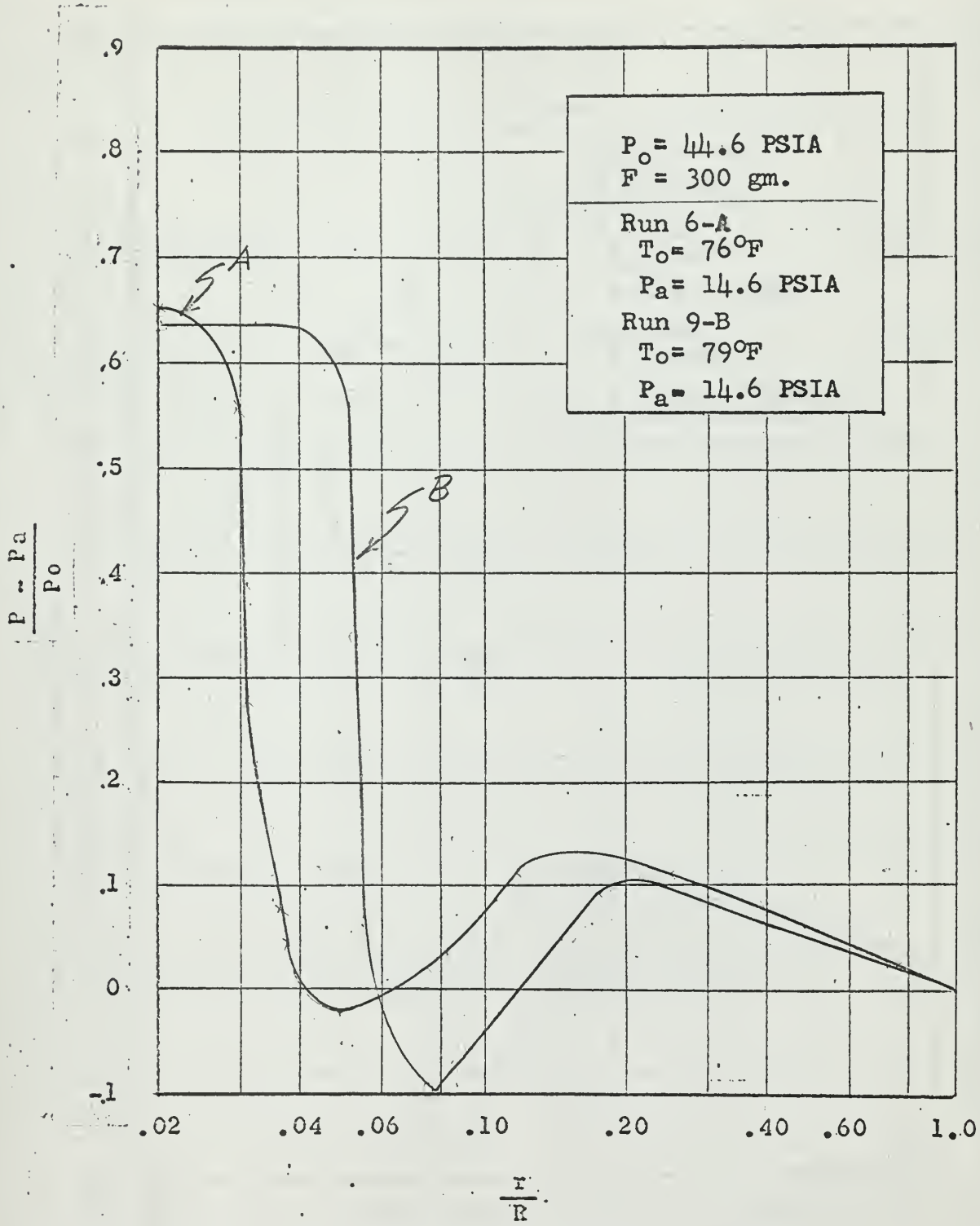

Fig. 5 - Plot of non-dimensional pressure versus radius ratio

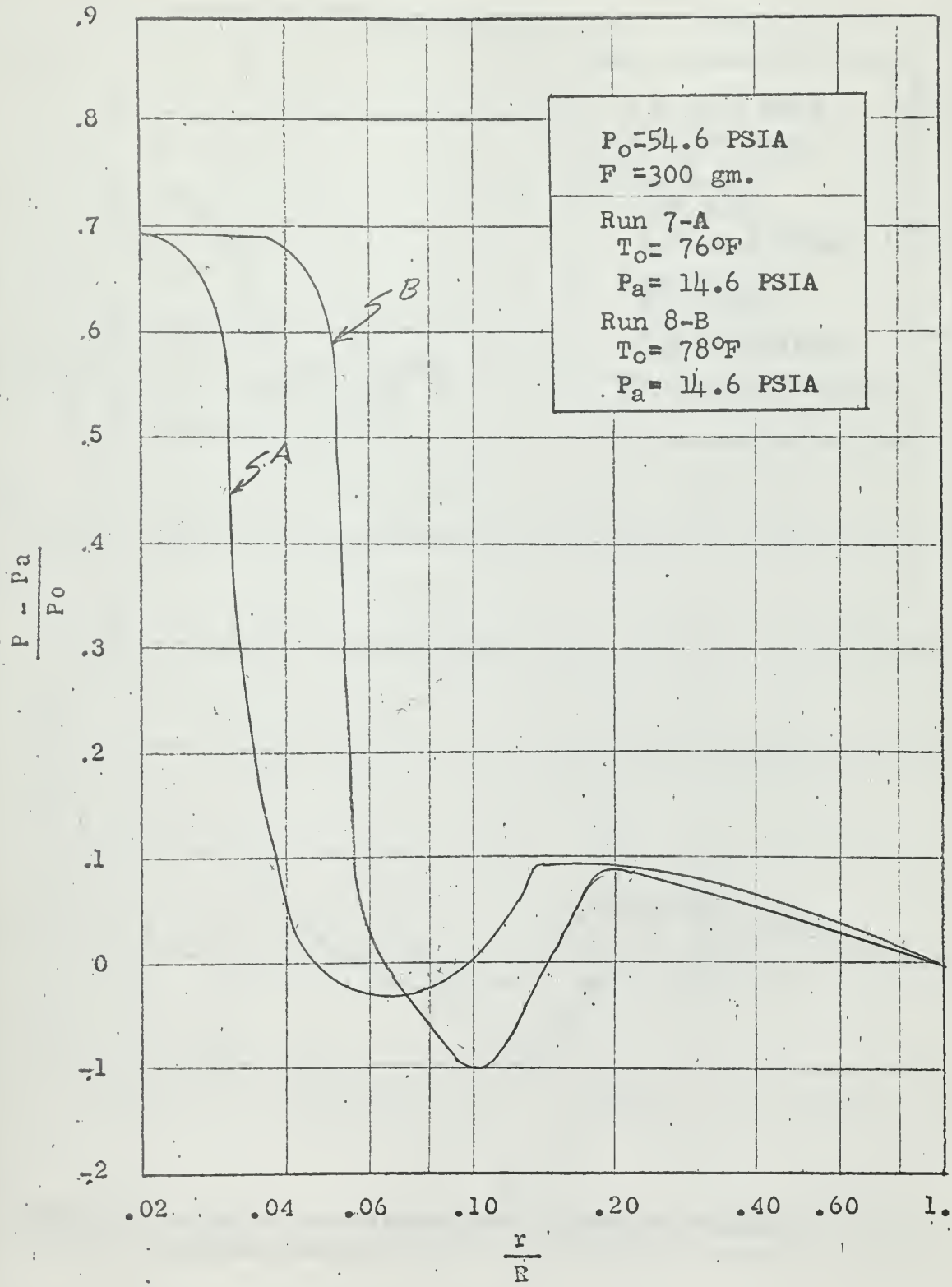

Fig. 6 - Plot of non-dimensional pressure versus radius ratio

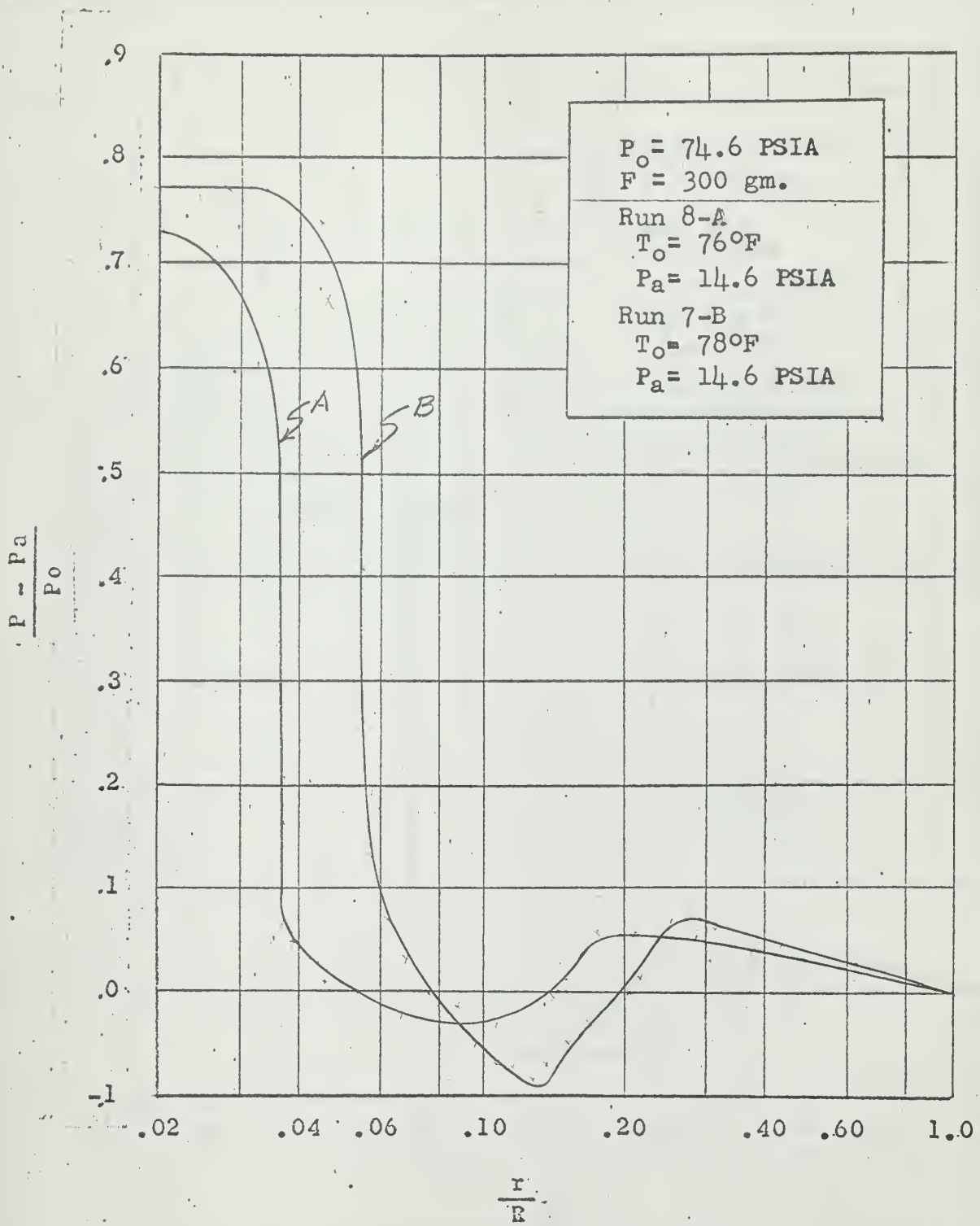

Fig. 7 - Plot of non-dimensional pressure versus radius ratio

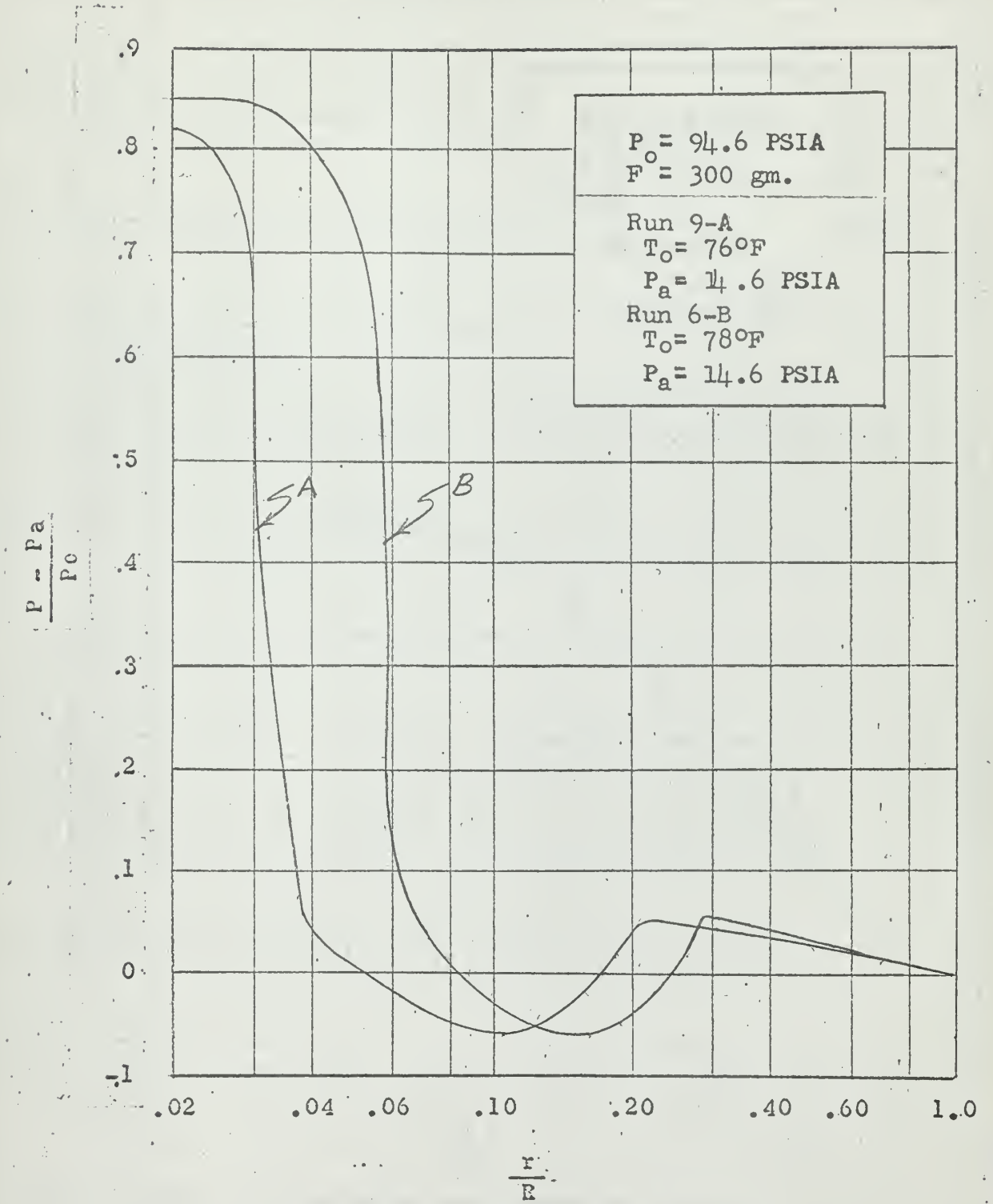

Fig. 8 - Plot of non-dimensional pressure versus radius ratio

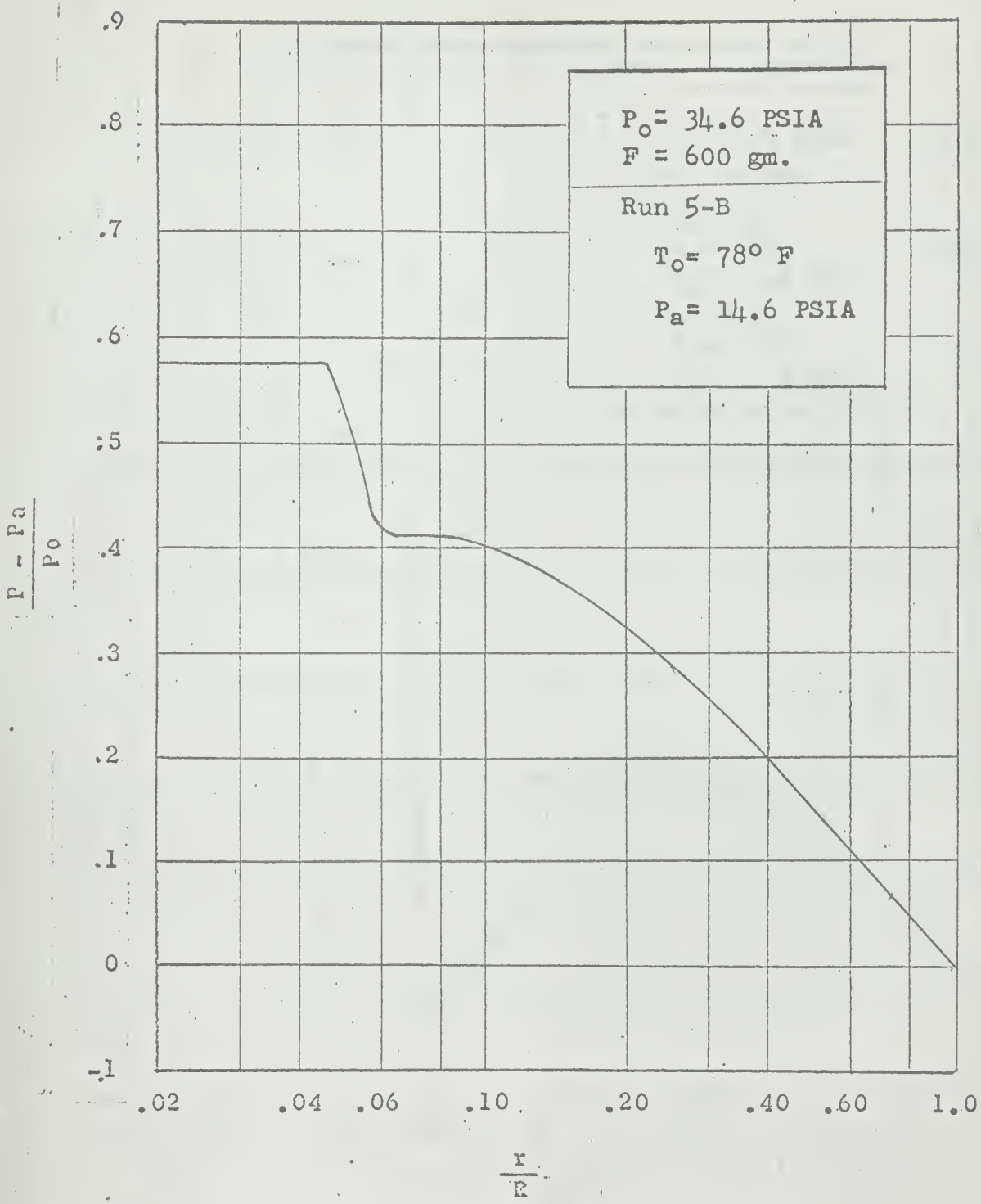

Fig. 9 - Plot of non-dimensional pressure versus radius ratio

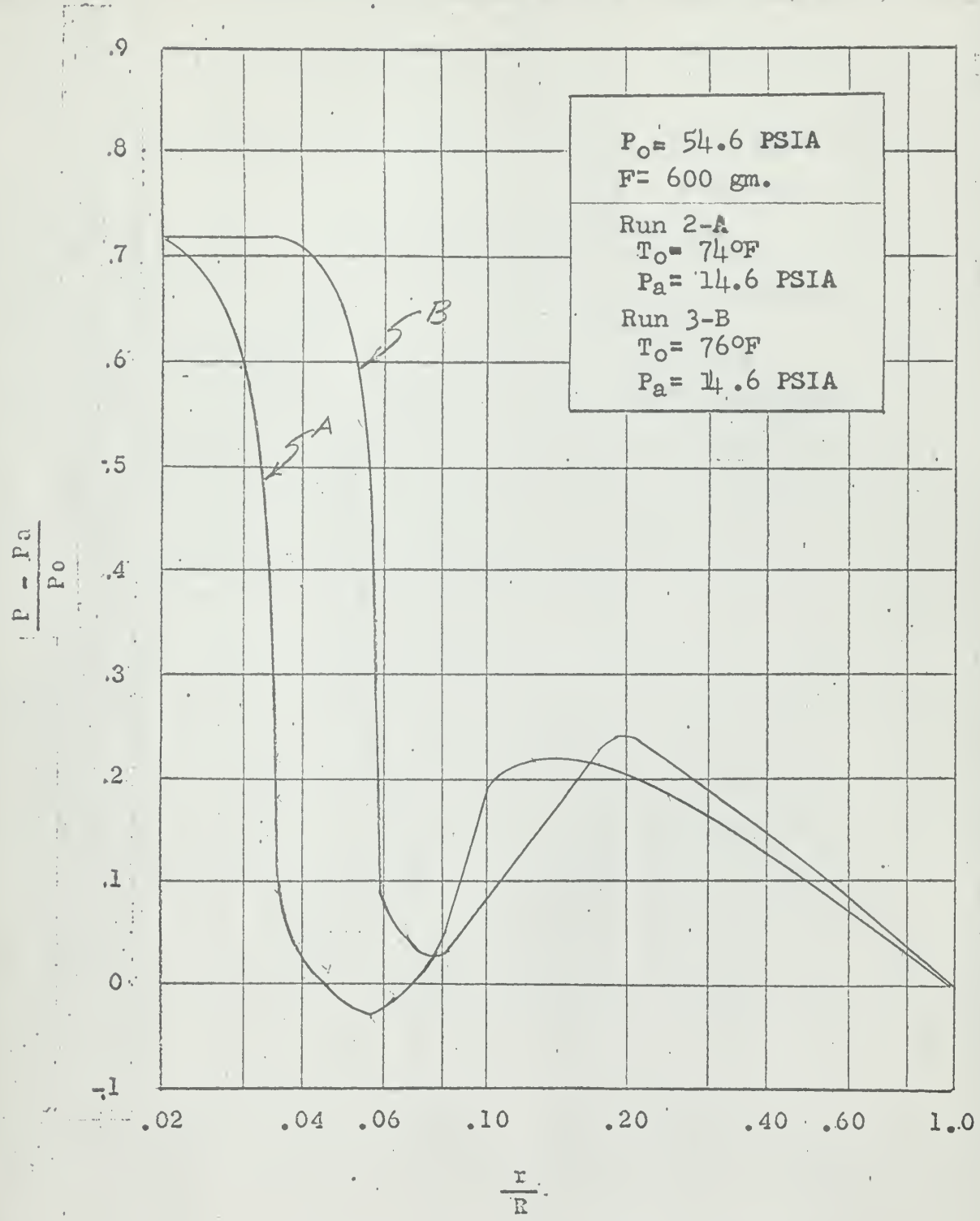

Fig. 10 - Plot of non-dimensional pressure versus radius ratio

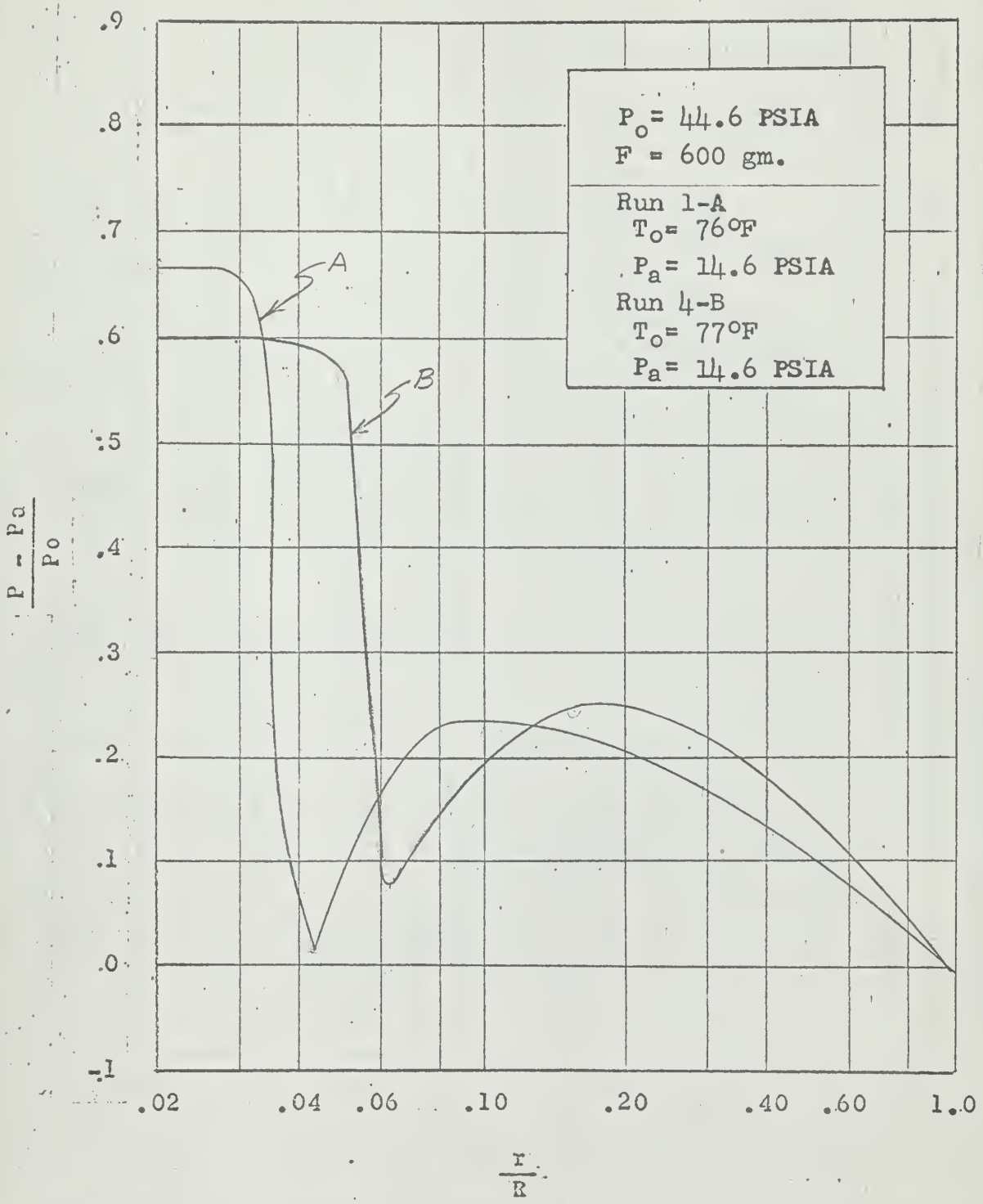

Fig. 11 - Plot of non-dimensional pressure versus radius ratio

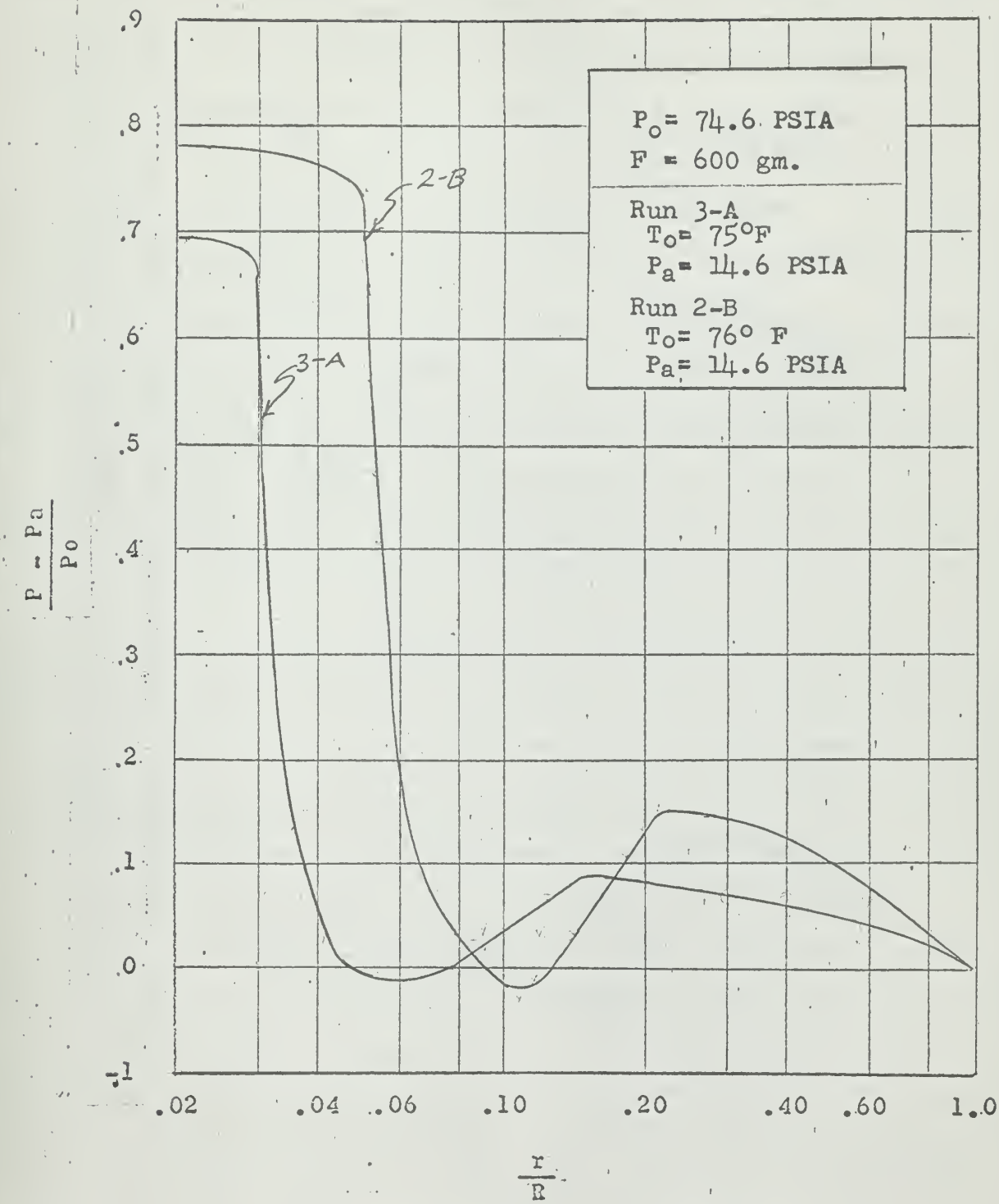

Fig. 12 - Plot of non-dimensional pressure versus radius ratio

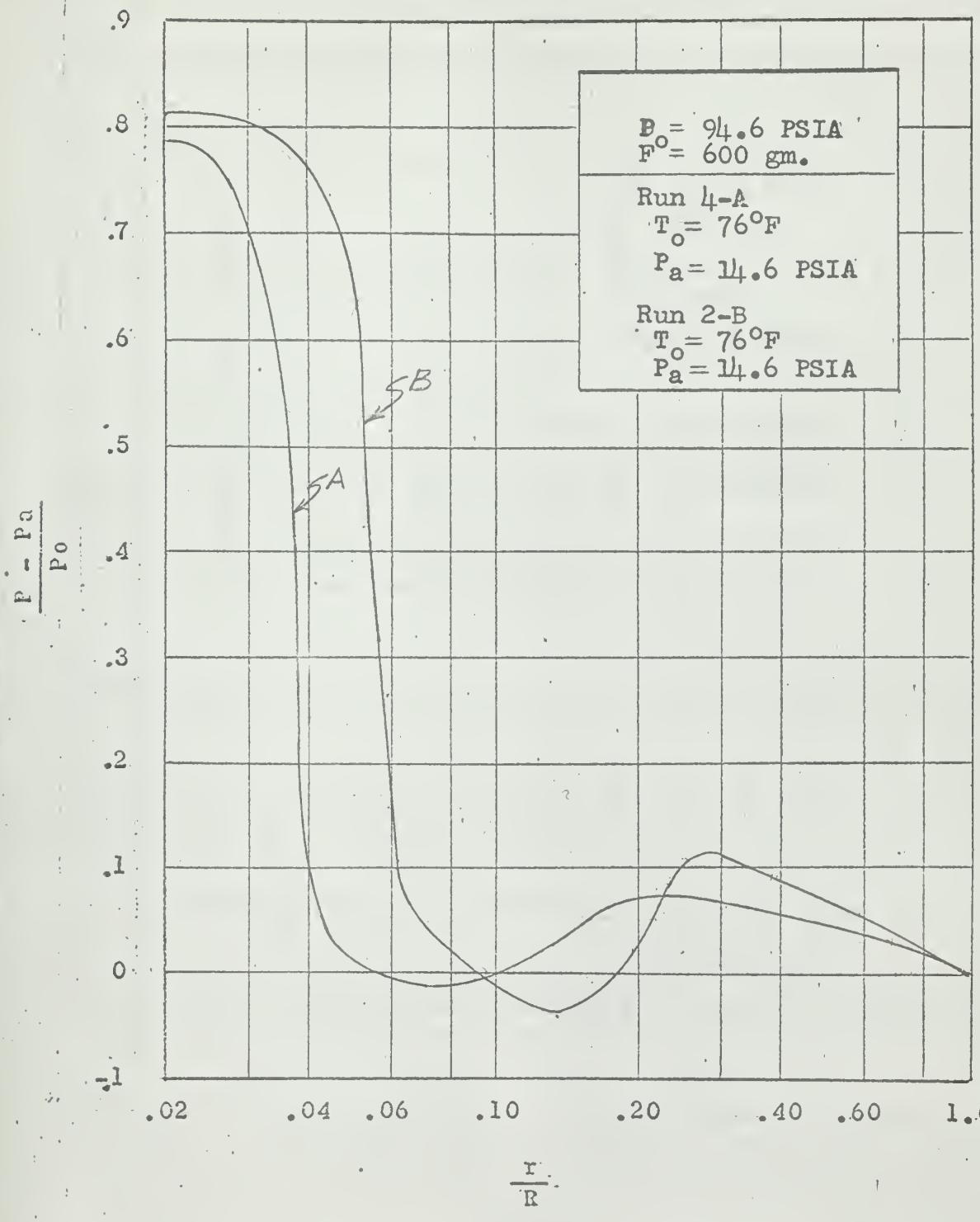

Fig. 13 - Plot of non-dimensional pressure versus radius ratio

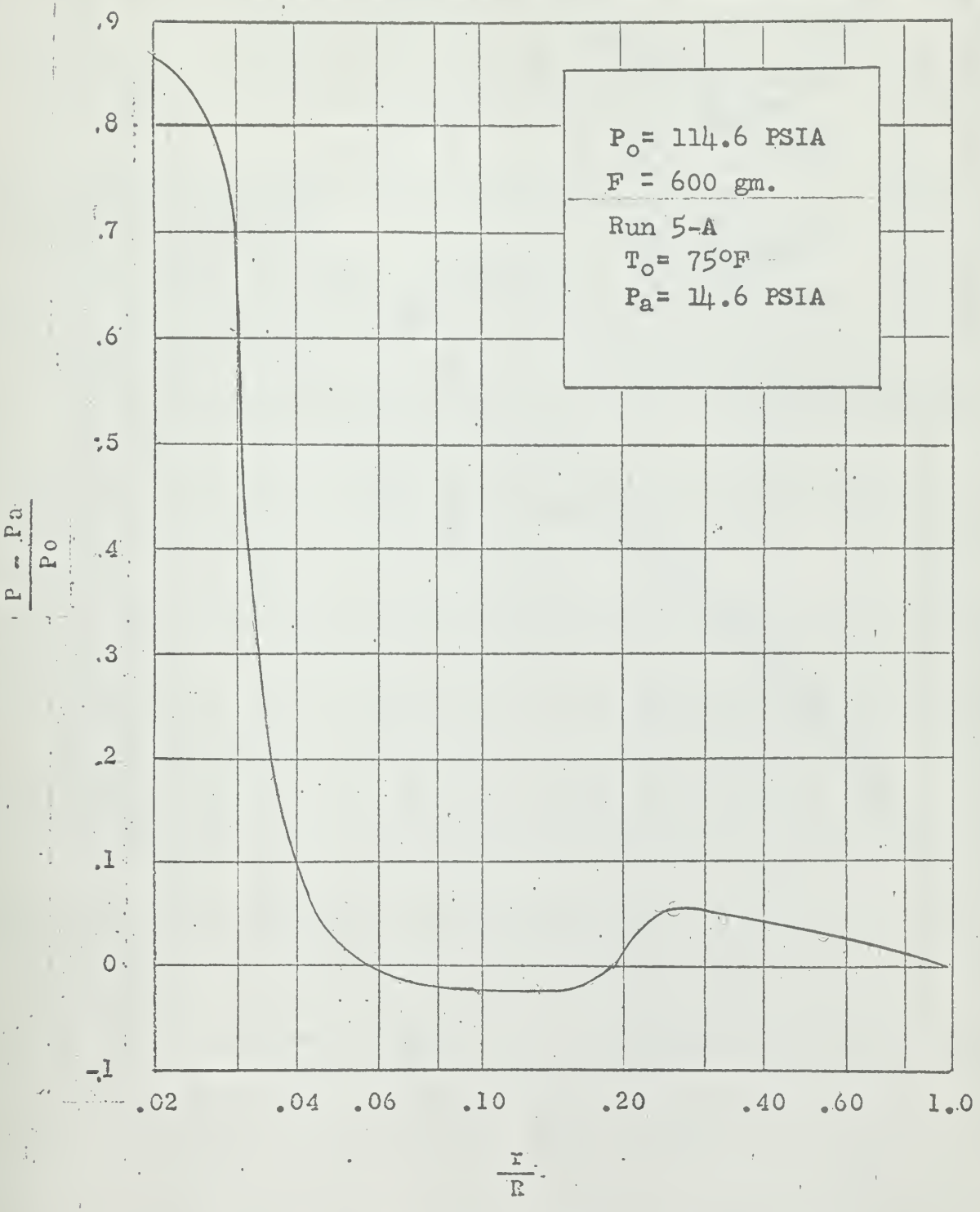

Fig. 14 - Plot of non-dimensional pressure versus radius ratio

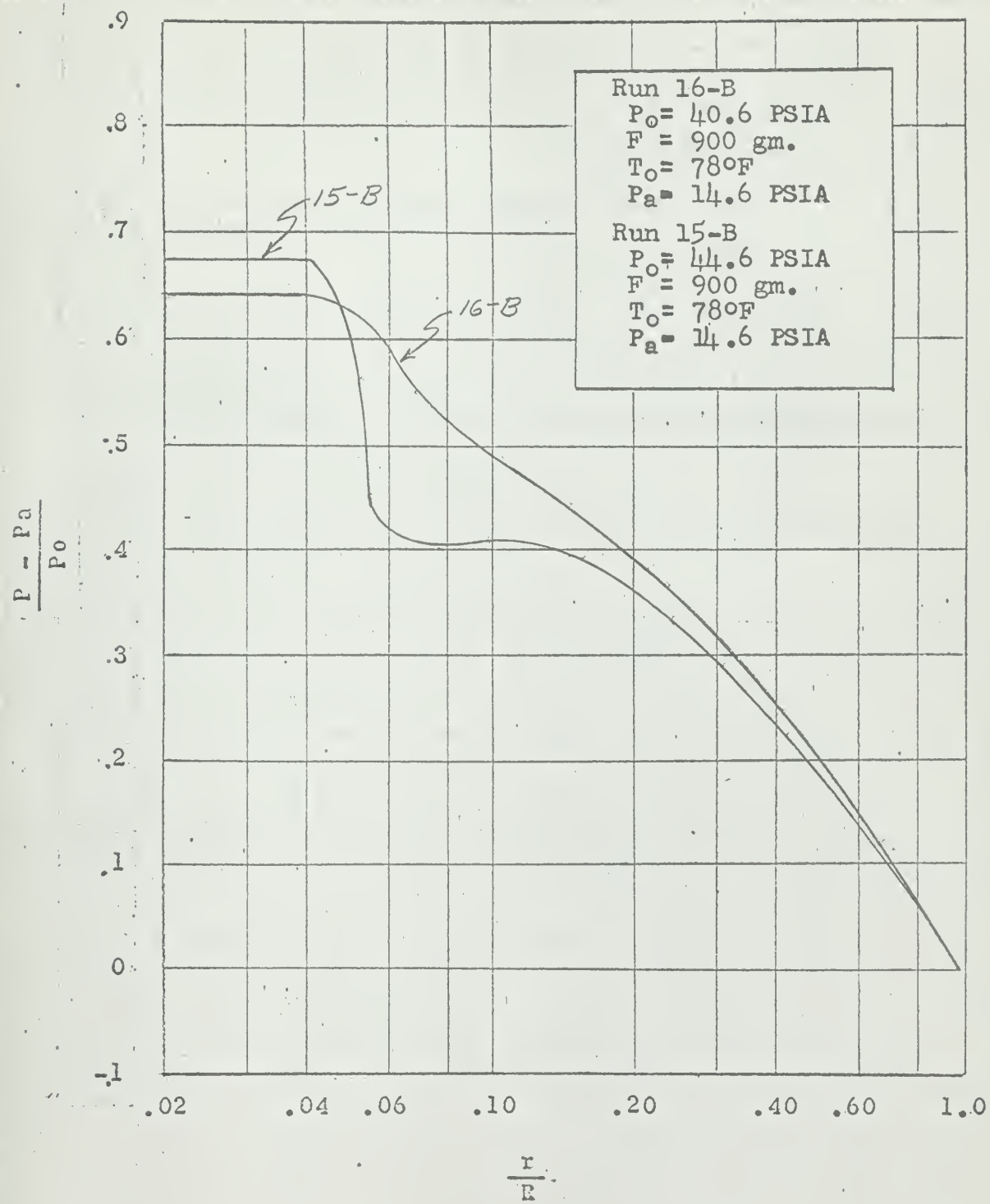

Fig. 15 - Plot of non-dimensional pressure versus radius ratio

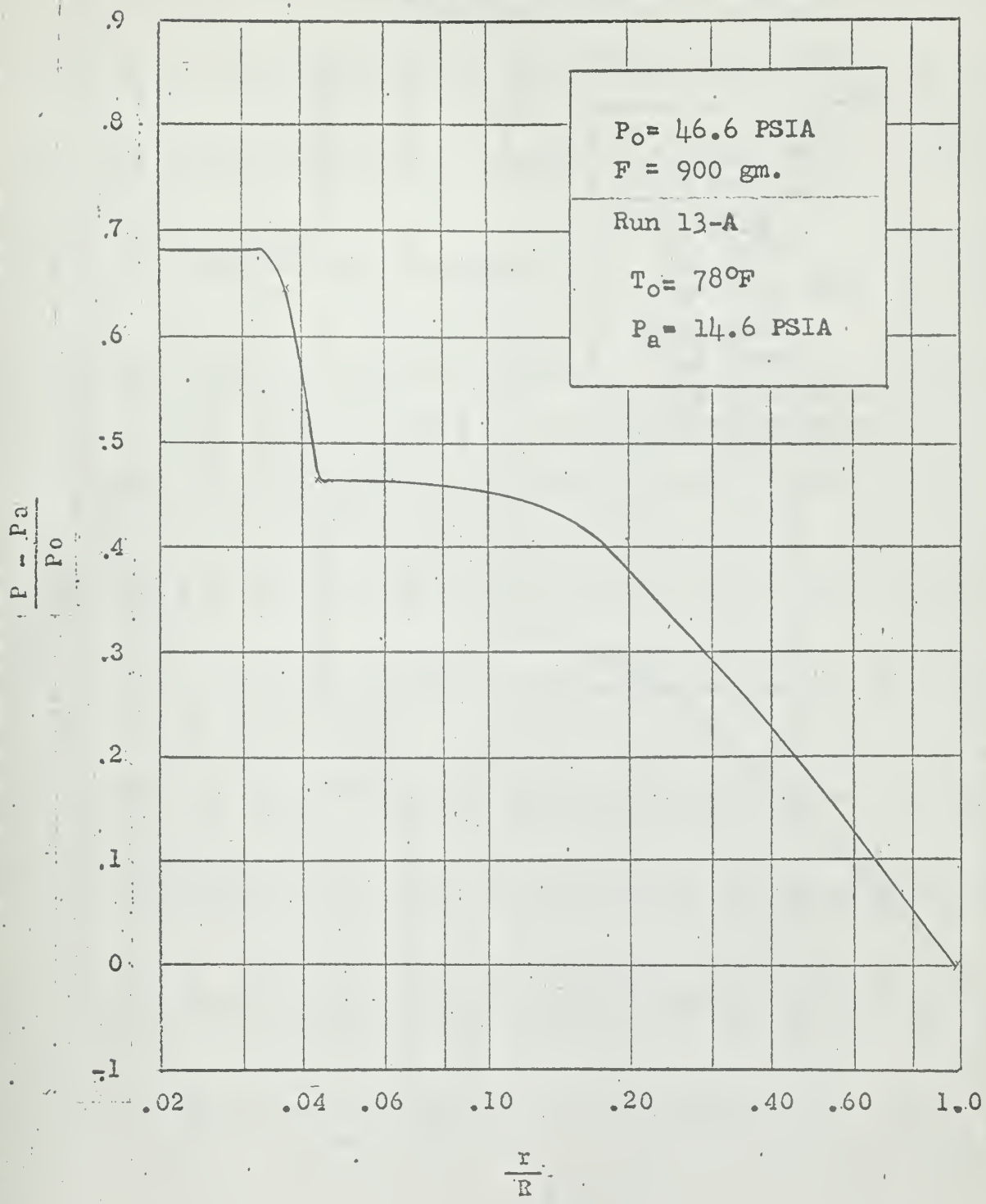

Fig. 16 - Plot of non-dimensional pressure versus radius ratio

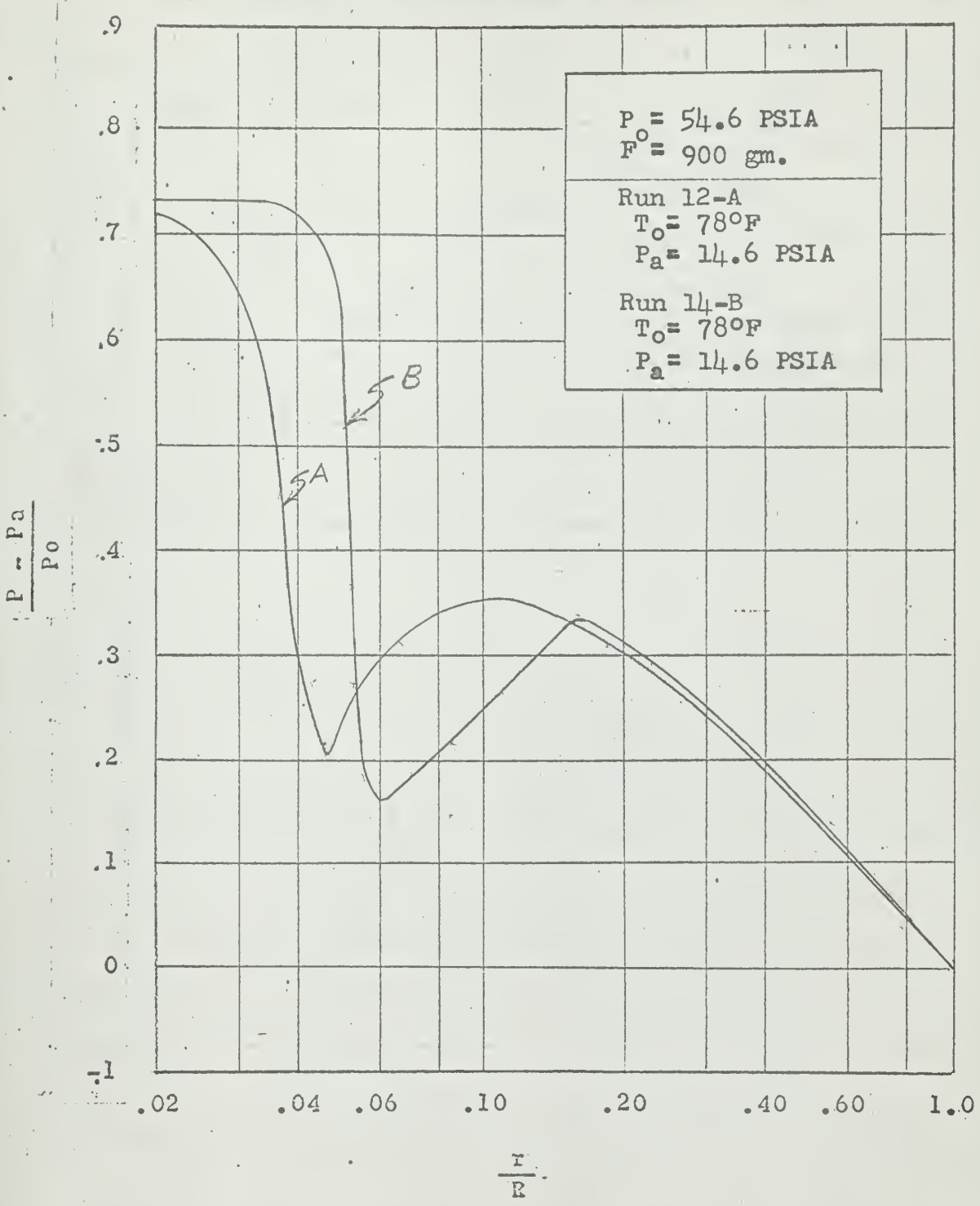

Fig. 17 - Plot of non-dimensional pressure versus radius ratio

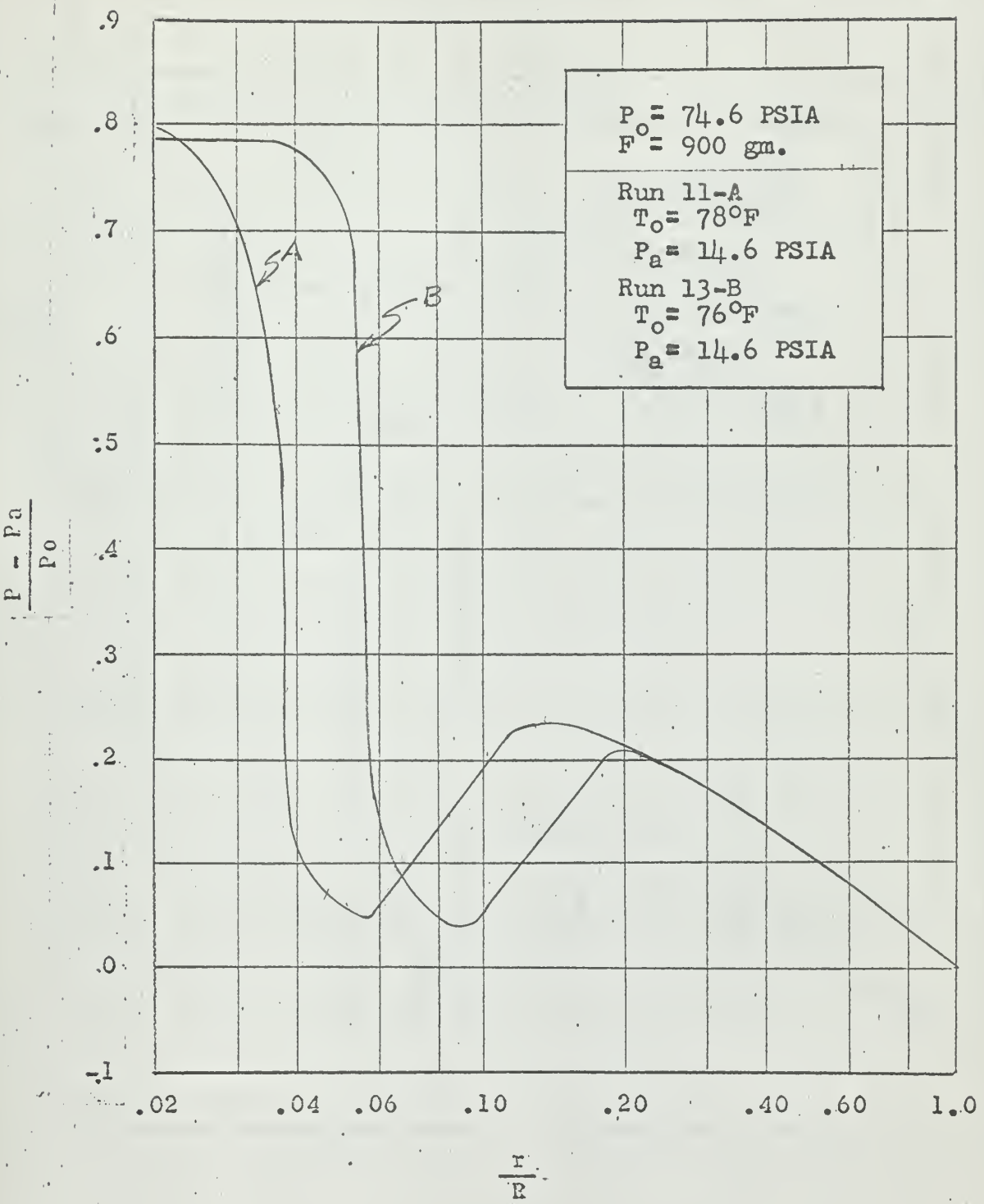

Fig. 18 - Plot of non-dimensional pressure versus radius ratio

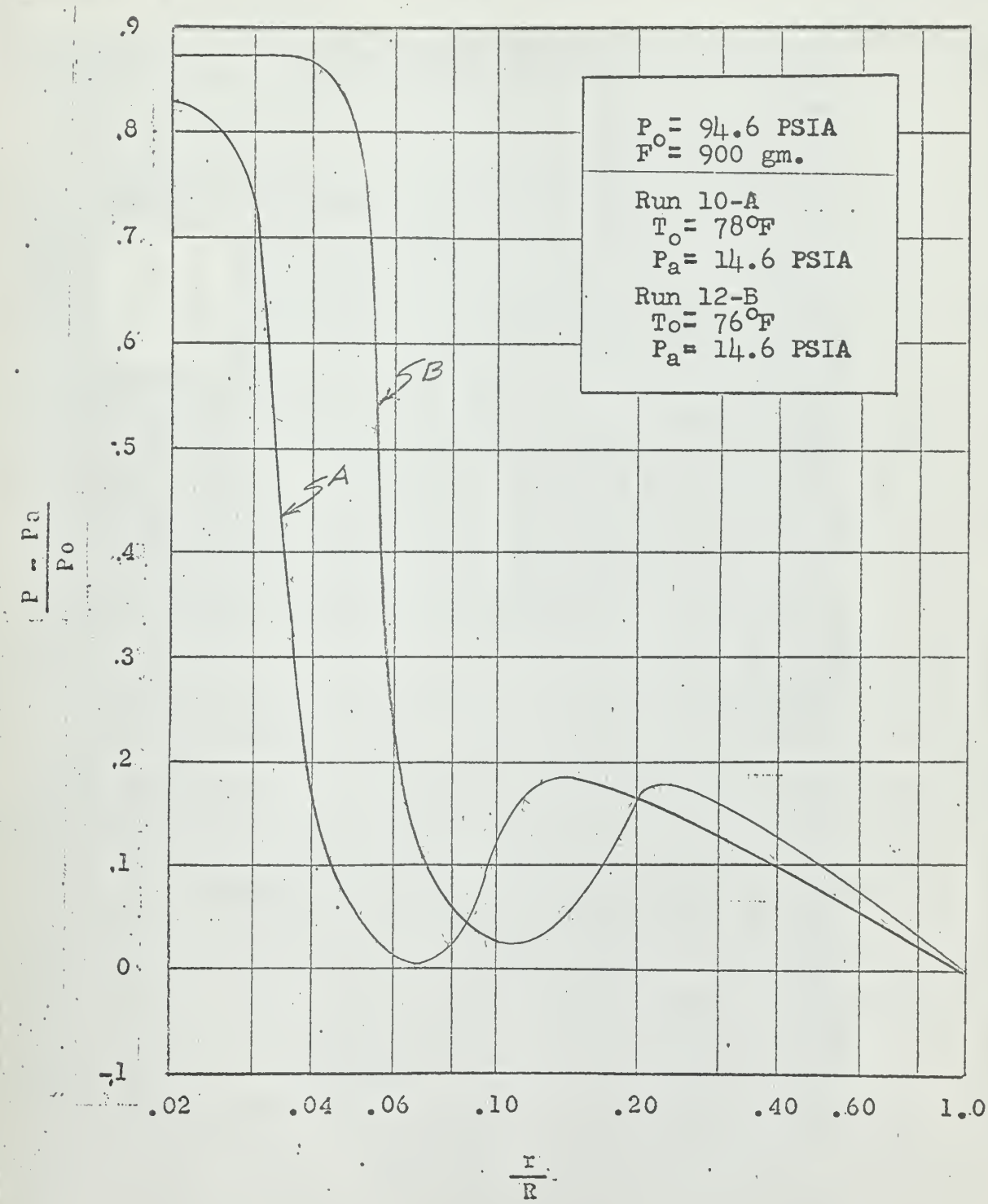

Fig. 19 - Plot of non-dimensional pressure versus radius ratio

Fig. 20 - Plot of pressure versus radius made by X-Y plotter

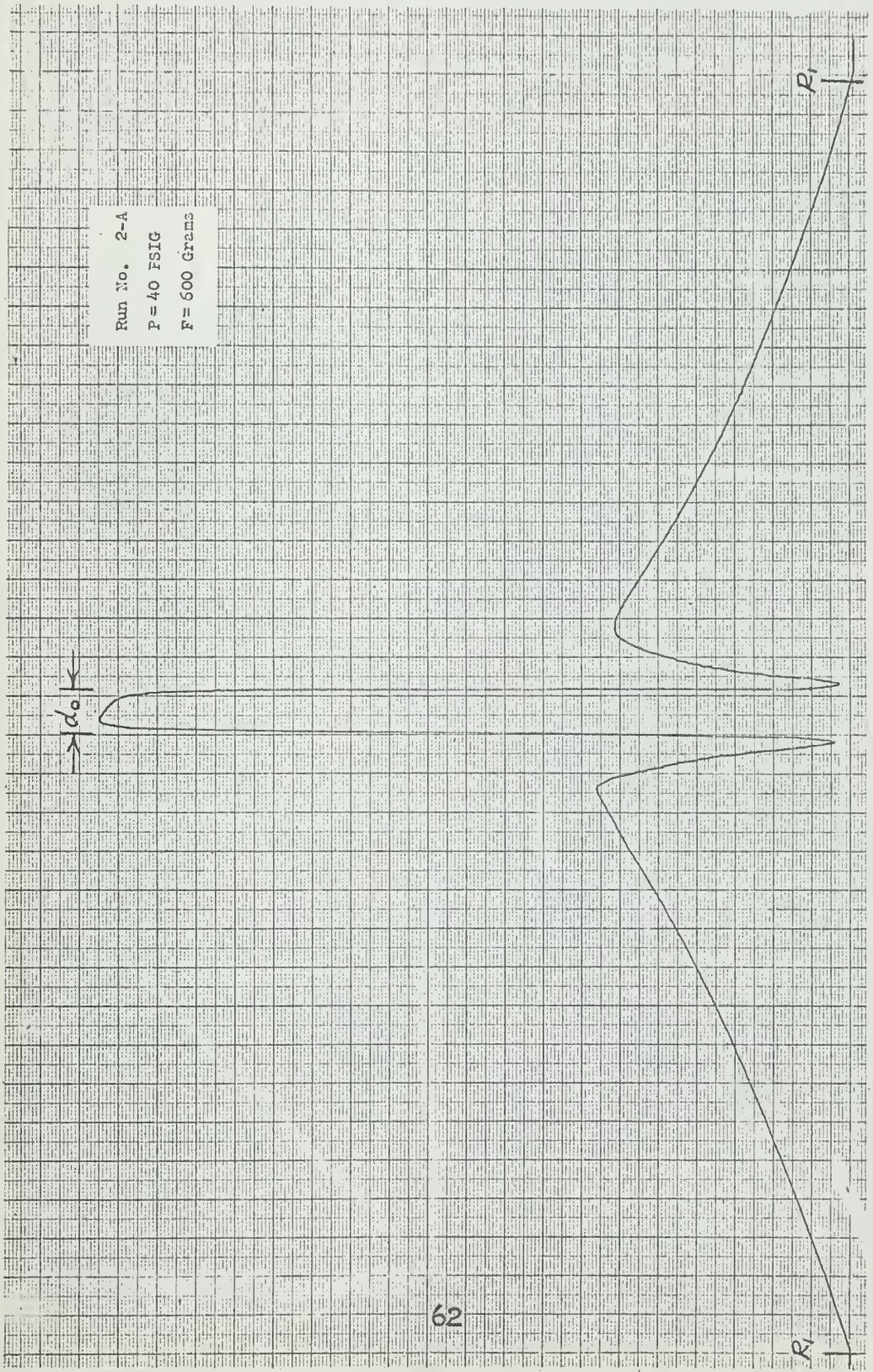

Fig. 21 - Plot of pressure versus radius made by X-Y plotter

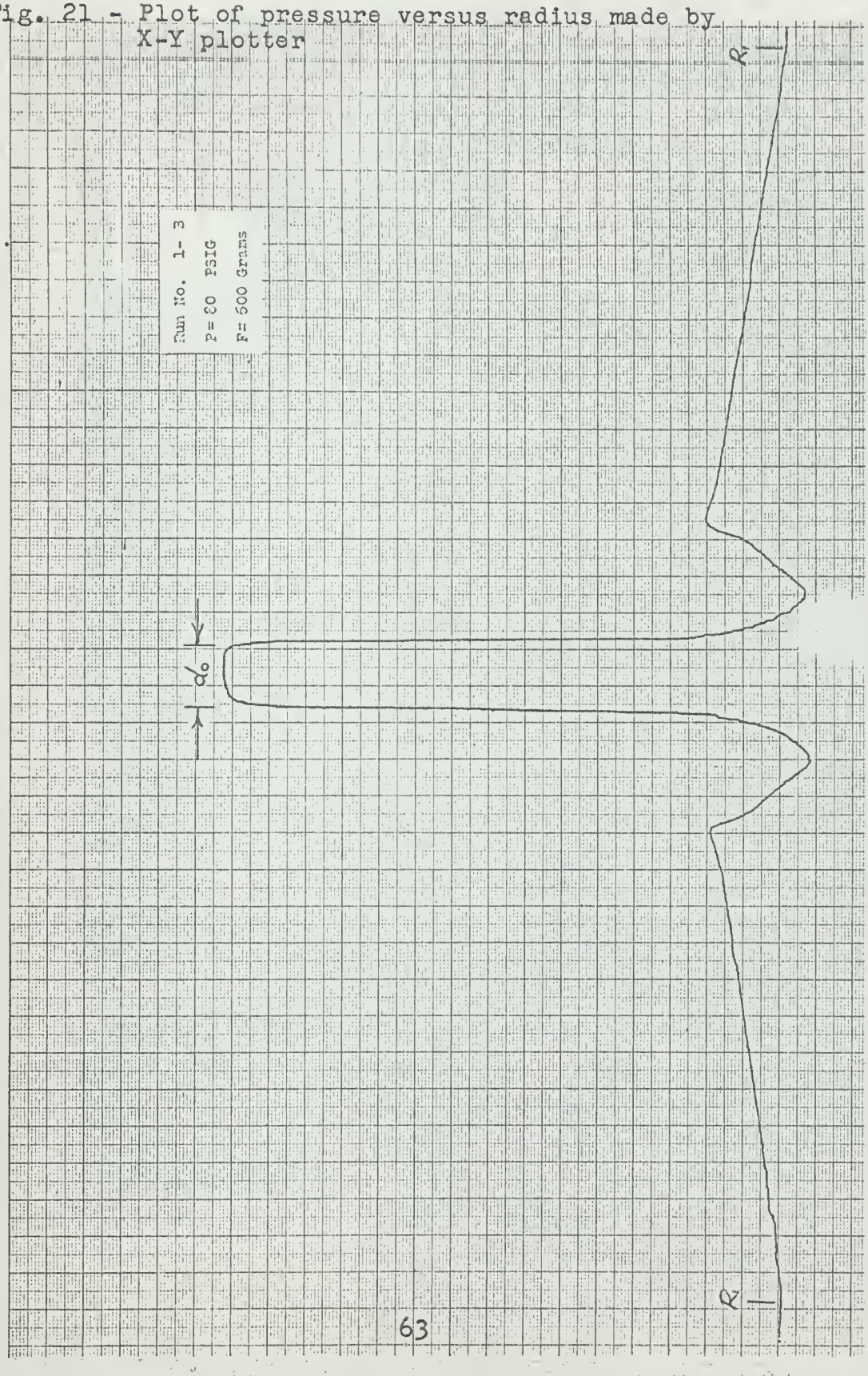

Fig. 22 - Plot of pressure versus radius made by X-Y plotter

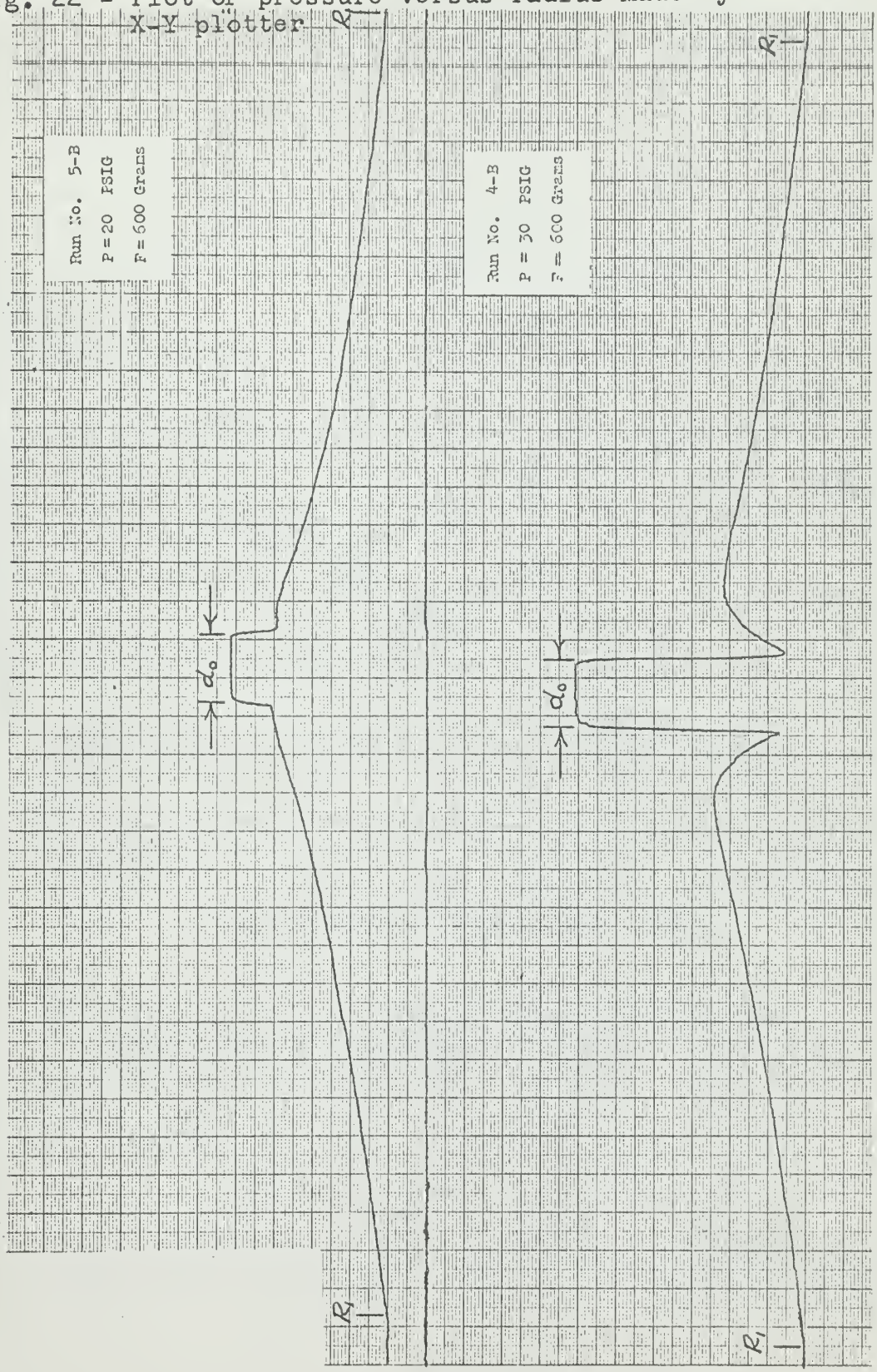

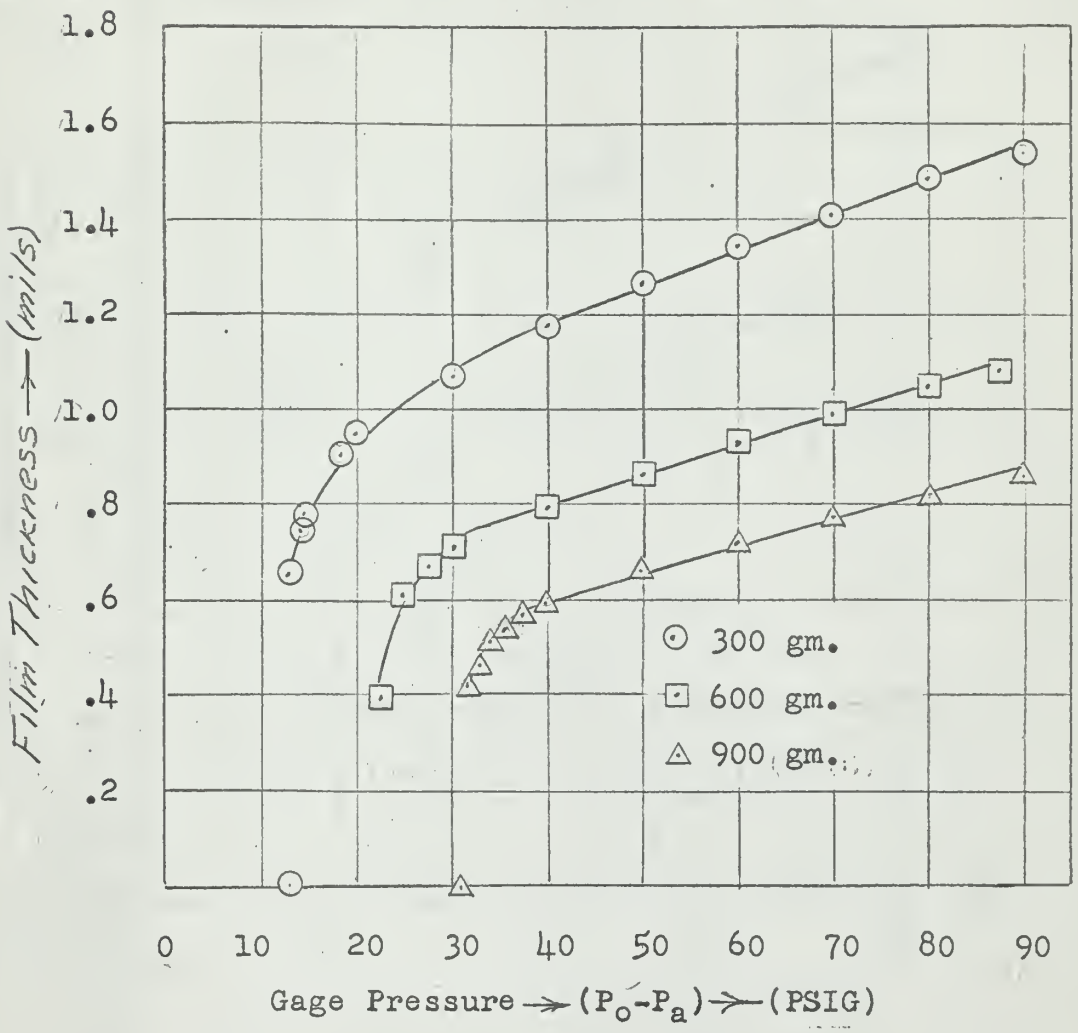

Fig. 23 - Plot of film thickness versus differential pressure for "A" head

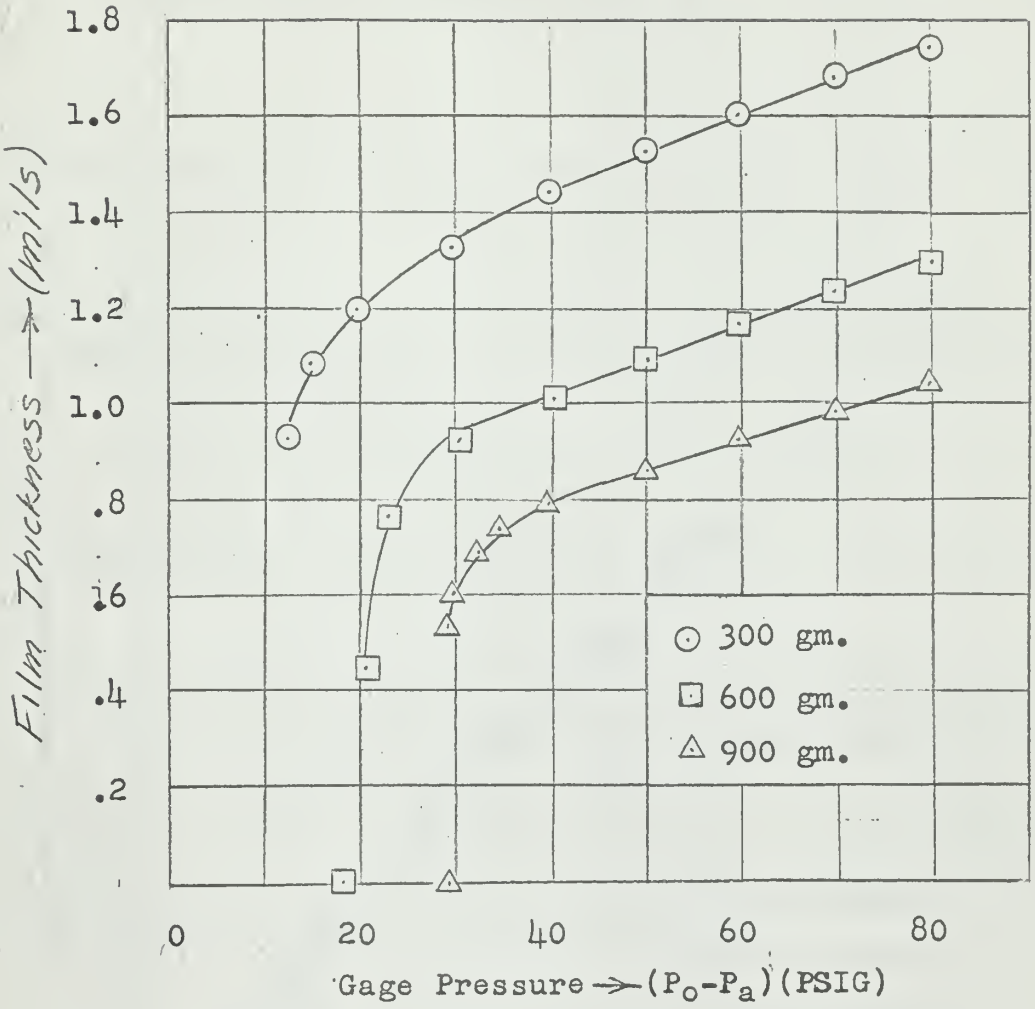

Fig. 24 - Plot of film thickness versus differantial pressure for "B" head

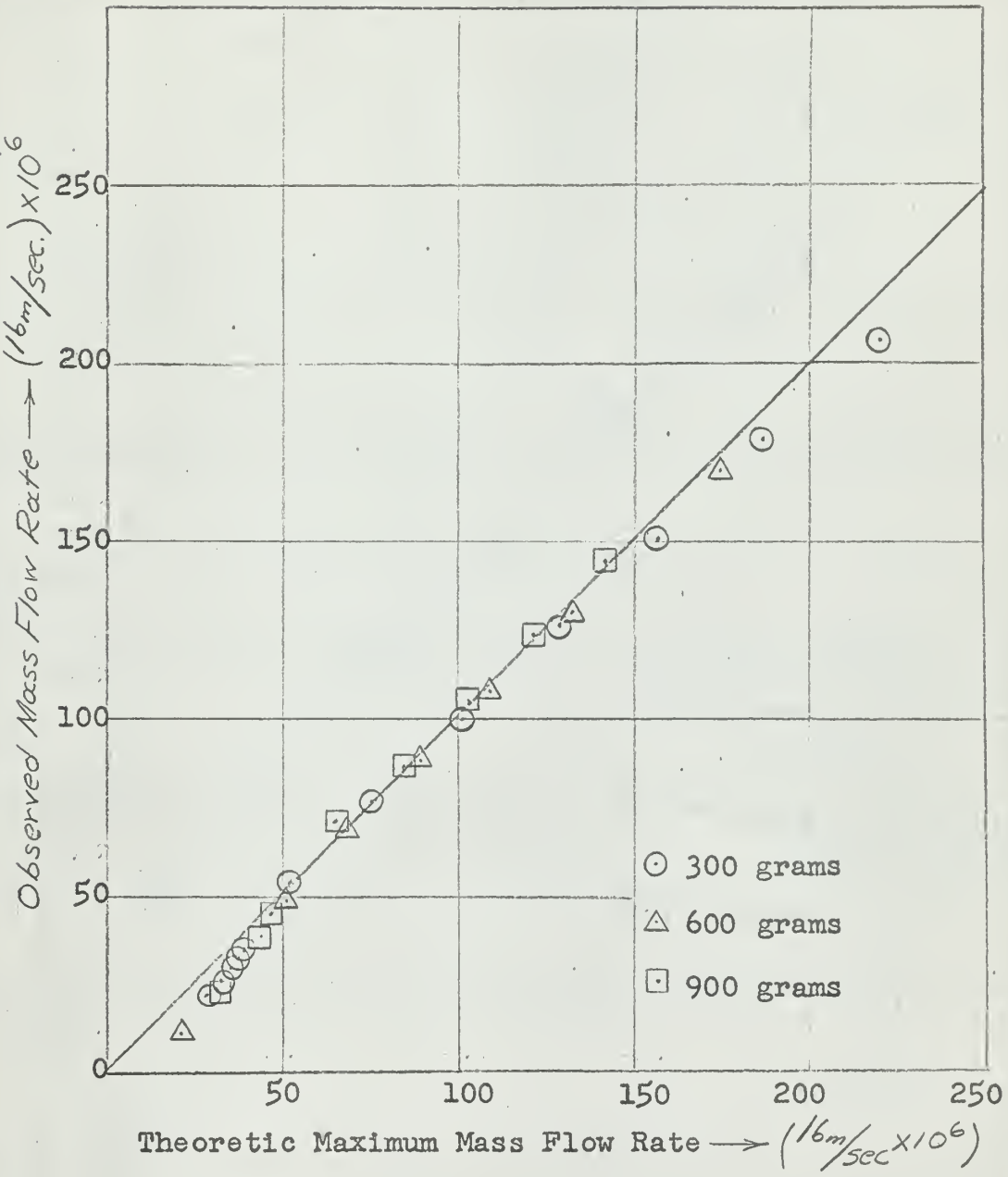

Fig. 25 - Plot of observed mass flow rate of air versus theoretic maximum mass flow rate of air for "A" head

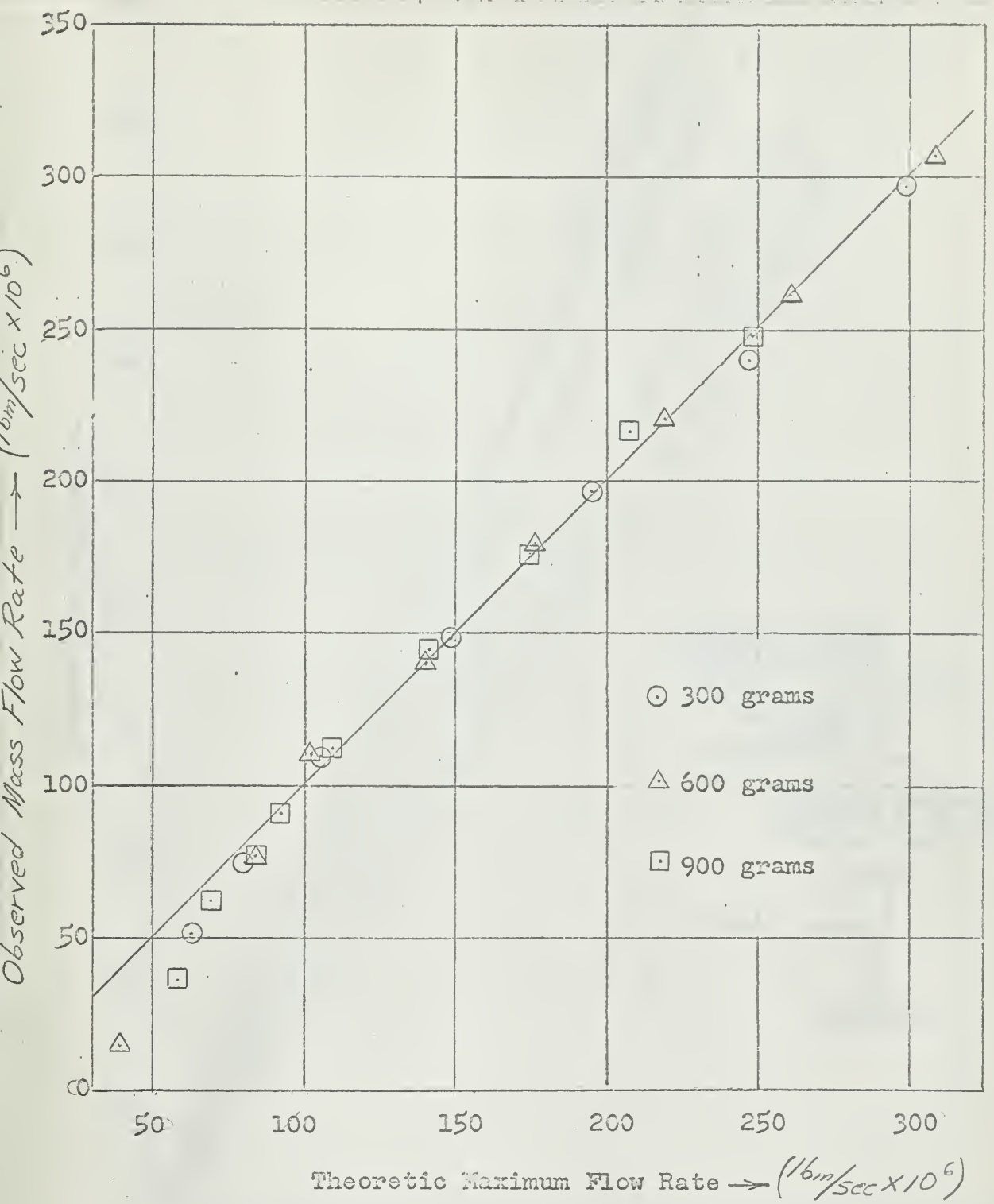

Fig. 26 - Plot of observed mass flow rate of air versus theoretic maximum mass flow rate of air for "B" head

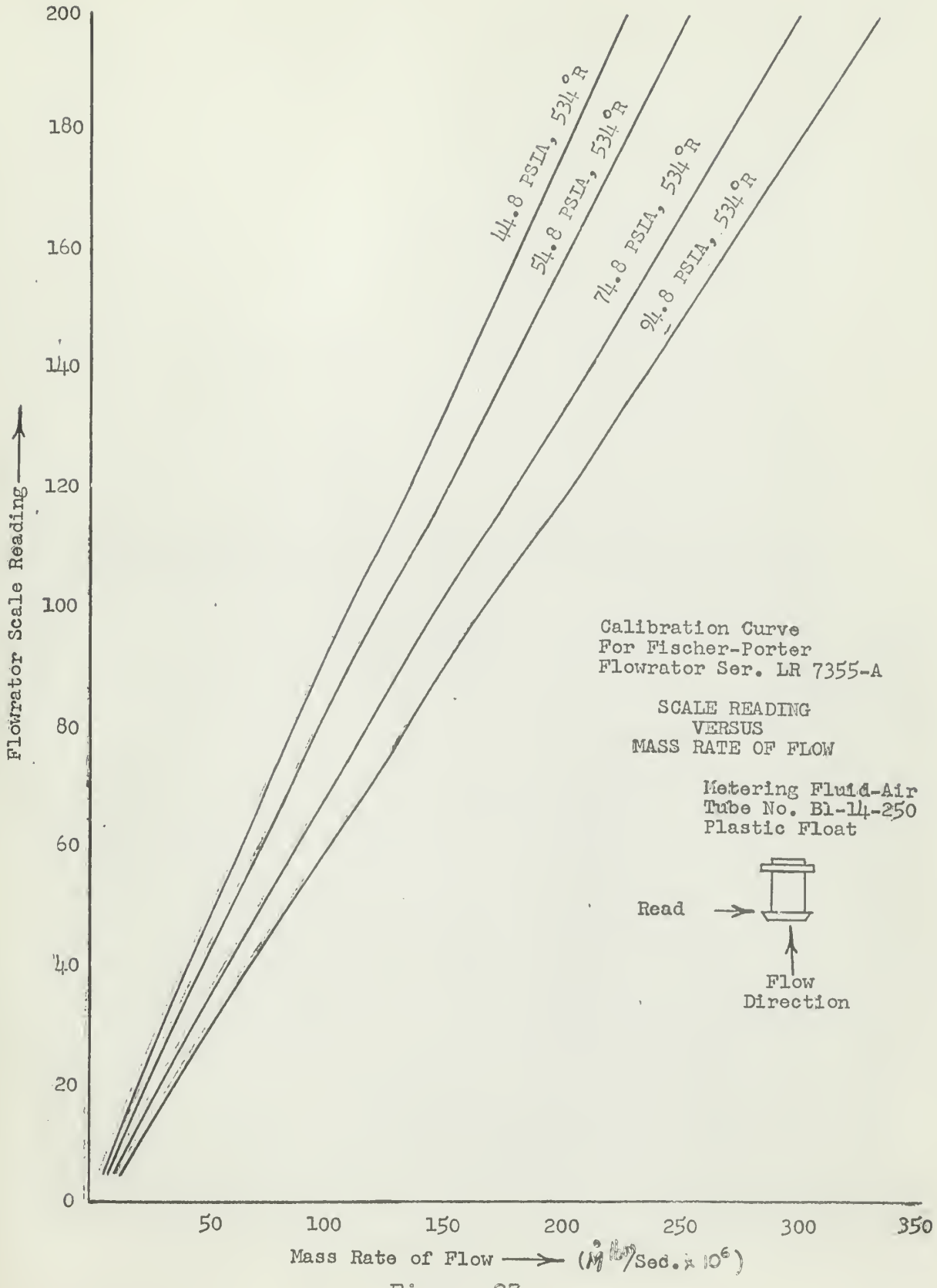
200
180
160
140
120
100
80
60
40
20
0
Flowrator Scale Reading
14.8 PSIA, 534 °R
54.8 PSIA, 534 °R
74.8 PSIA, 534 °R
94.8 PSIA, 534 °R
Calibration Curve
For Fischer-Porter
Flowrator Ser. LR 7355-A
SCALE READING
VERSUS
MASS RATE OF FLOW
Metering Fluid-Air
Tube No. B1-14-250
Plastic Float
Read
Flow
Direction
50
100
150
200
250
300
350
Mass Rate of Flow → (lbm/Sec. x 10^6)

Figure 27